AIAA-2000-2391

ASSESSMENT OF CFD PREDICTIONS OF VISCOUS DRAG

Brenda M. Kulfan
Boeing Commercial Airplane Group
Seattle, Washington

Fluids 2000
19-22 June 2000 / Denver, CO

AIAA-2000-2391

ASSESSMENT OF CFD PREDICTIONS OF VISCOUS DRAG

Brenda M. Kulfan*
Boeing Commercial Airplane Group
Seattle, Washington

ABSTRACT

Recent CFD design and analyses studies have shown significant variations in viscous drag predictions for a typical High Speed Civil Transport configuration. The sensitivity of the design of an HSCT configuration to cruise drag is discussed. Results of the first two-phases of a five-phase program defined to resolve the observed drag prediction differences are shown. The first phase involved the formulation of an experimental database of fully turbulent flow flat plate skin friction measurements at subsonic through supersonic Mach numbers and for a wide range of Reynolds numbers. Statistical analyses of the data were conducted to establish meaningful skin friction equations to represent the database for use in evaluating the viscous drag predictions by various Navier Stokes codes. Improved flat plate skin friction prediction equations that matched the mean of the skin friction database values were developed in the process. Boundary layer profile data measurements are included along with a refined method for predicting boundary layer growth characteristics. In phase two, CFD flat plate viscous drag predictions were made using a number of different Navier Stokes codes, analyses schemes and participating organizations. Comparisons of Navier Stokes CFD skin friction predictions indicate significant variations between the various CFD predictions and also with the test data.

* Boeing Technical Fellow Aerodynamics
Mail stop 67-LF
brenda.m.kulfan@boeing.com

INTRODUCTION

The design of a viable High Speed Civil Transport, HSCT, configuration is very sensitive to the aerodynamic design features and the associated cruise drag characteristics. A one percent reduction in supersonic cruise drag, which is approximately 1 drag count (CD ~ 0.0001) has the following impact on a configuration sized to meet typical HSCT design objectives:

- Reduces Airplane Gross Weight by 10,000 pounds
- Saves 7,500 Pounds of Fuel
- Is Equivalent to a 2,000 Pound Reduction in Structural Weight

At high subsonic cruise conditions, (Mach ~0.90 to 0.95), 1 count of drag has about ¼ the impact of 1 count of supersonic cruise drag. Relatively small changes in drag can therefore greatly impact the design selection and definition of the features of an optimized configuration arrangement. This is particularly important if decisions have to be made on predicted relative performance benefits between various design options.

Figure 1 illustrates many of the design features for a typical HSCT. The definition of each of these design features involves design trade studies involving aerodynamics, structures and weight considerations, propulsion system, and systems design and along with relative benefits versus risk assessments.

The nature of the flow over the configuration and the effectiveness of the control surfaces can also be very dependent on the Reynolds Number as indicated in figure 2. This can affect many elements of the overall performance characteristics of the configuration.

The wind tunnel is used in conjunction with the emerging CFD design and analysis tools in the aircraft design process as well as in the generation of the performance database. As shown in Figure 3, the

current wind tunnel capabilities are unable to represent full-scale conditions for an HSCT configuration. Two options are generally available to the aerodynamist:

1. Use the wind tunnel to validate and calibrate the CFD methods. The CFD methods are used to predict full scale conditions. This is the typical design process approach.
2. Calibrated CFD methods are used to extrapolate the wind tunnel data to full scale conditions. This is typically the approach to generate the extensive performance database required for the development of a commercial aircraft configuration.

Either approach leads to a number of fundamental Reynolds Number related questions:

- Are correct configuration decisions being made?
- Are the correct high lift systems and control surfaces being developed?
- When is testing at low Reynolds adequate?
- When is testing at high Reynolds number required?
- Can CFD codes, validated with low Reynolds number data, adequately predict forces, moments and flow characteristics at full-scale conditions?
- Can errors between measured and predicted drag levels mean incorrect representation of the flow physics?

During Recent HSCT design studies significant variations in the viscous drag predictions were obtained by different organizations and with alternate turbulence models, as shown in Figure 4, for an HSCT wind tunnel model wing plus body configuration. There were substantial differences in flat plate theory predictions used in the inviscid CFD analyses and also between the CFD predictions obtained with the viscous analyses. This posed a concern since each organization was developing optimized configurations using their favored CFD tools. IF the tools produced different answers on a common analysis configuration, how valid would comparisons be of different design options predicted by the different codes?

Similar differences between viscous drag predictions using different turbulence models and flat plate skin friction have been observed by Melissa Rivers and Richard Wahls[19]. Figures 5 through 7 contain data and results from their assessments of various turbulence models applied to the analysis of a typical HSCT configuration. Figure 5 contains a comparison of an experimental wind tunnel model drag polar with CFD drag predictions using four different turbulence models. The differences between the theoretical predictions and the measured drag level at an angle of attack of 5 degrees are also shown. The theoretical predictions were all substantially less then the test data. Theory under predicted the measured drag by 8 to 15 drag counts (-0.0008 to –0.0015).

Figure 6 contains comparisons of the CFD predictions of the viscous drag for the model with estimates made using flat plate theory. The differences between the CFD predictions of the viscous drag and the flat plate viscous drag as shown in this figure are very similar to the test versus theory differences shown in figure 5. The CFD predictions fall from 12.5% to 28.1% lower then the flat plate predictions of the viscous drag.

The drag polar predictions with the CFD viscous drag predictions replaced by the flat plat theory nearly match the test data exactly as shown in Figure 7. Hence, it was felt that an important element, in validating the viscous drag predictions of any Navier Stokes code, is to make sure that predictions of the local and average skin friction drag and boundary layer must match the "simple" flat plate measured skin friction test data over the range of Mach numbers and Reynolds for which the codes will be used. This process should help to evaluate the applicability of the various turbulence models. The validated codes and calculation schemes could then be applied to increasingly more sophisticated configuration geometry. A strategy was developed to help resolve the differences in the observed on the viscous drag predictions for an HSCT configuration. Results of first two phases will be shown in this report.

The first phase[1], involved the formulation of an experimental database of fully turbulent flow skin friction measurements on flat plate adiabatic surfaces at subsonic through supersonic Mach numbers and for a wide range of Reynolds numbers. Statistical analyses of the data were conducted to establish appropriate skin friction equations to represent the database for use in evaluating the viscous drag predictions by various Navier Stokes codes. Improved flat plate skin friction prediction equations that matched the mean of the skin friction database values were developed in the process.

Boundary layer profile data measurements were also included and were used to develop a refined method for predicting boundary layer growth characteristics. These include approximate velocity profile representation, boundary displacement thickness, and boundary layer thickness.

In the second phase[2], CFD flat plate viscous drag predictions were made using a number of different Navier Stokes codes, analysis schemes and participating organizations. These included Boeing Phantom Works, Long Beach, (BPW-LB); NASA Ames Research Center, (ARC) and Boeing Commercial Airplane Group in Seattle, (BCAG). The Boeing Long Beach predictions were made by Hamid Jafroudi of Alpha Star Corp, the NASA Ames calculations were made by Scott Lawrence and the Boeing Seattle calculations were made by Max Kandula of Dynacs.

Comparisons of Navier Stokes CFD skin friction will be presented along with detailed analyses of the results. The study conclusions will be summarized.

EXPERIMENTAL SKIN FRICTION DATA BASE

The objective was to obtain an experimental database of fully turbulent flow skin friction measurements on flat plate adiabatic surfaces at subsonic through supersonic Mach numbers and for a wide range of Reynolds numbers. The database would then be used as the initial step in resolving the differences in the CFD viscous predictions.

The database selected was originally assembled in 1960 from an extensive survey of selected experiments from many independent sources[3]. A rigid set of criteria had been adopted as a means of selecting appropriate test data for a systematic study. This was done to insure that the test conditions closely approximate the theoretical model, and that both the measurement and reduction techniques were such as to yield accurate and consistent information.

The most significant of these requirements were:

- Only data obtained by direct force measurements were used. Discussions of the relative merits of various skin friction measurement techniques indicated that the most accurate data are obtained by direct force measurements[4,5,6,7].
- The flow over the experimental model was to be properly tripped to satisfy the condition of fully turbulent flow.
- Measurements were to be made at stations far enough downstream of the trips to allow the flow to reach a "naturally" turbulent character.
- Experimental results were to be presented in terms of the properly determined effective turbulent length. The effective turbulent length corresponds to the length of fully turbulent flow that produces the same flow characteristics as the flow characteristics at the experimental measuring station.

It was felt that the use of the existing database represented an extensive and meaning set of readily available data that could be used to assess the CFD predictions.

The experimental data also included turbulent boundary layer velocity profiles and it was therefore possible to analyze other boundary layer properties such as shape factor, displacement thickness and boundary layer thickness. Boundary layer profile data measurements are also included along with a new method for predicting boundary layer growth characteristics. These include approximate velocity profile representation, boundary displacement thickness, and boundary layer thickness.

Flat plate skin friction drag predictions and boundary layer growth predictions have been found to be very useful for a number of preliminary design, PD, applications. Because typical HSCT configurations have rather thin wings, slender bodies and low cruise lift coefficients, experience has shown that flat plate skin friction calculations provide good estimates of the viscous drag. The predictions are easy, quick, robust and quite accurate. Current PD viscous drag prediction methods are often based on flat plate skin friction drag calculations. Often wind tunnel data is extrapolated to flight conditions using flat plate friction drag predictions.

Flat plate estimates of the boundary layer thickness have been used as the preliminary criteria for specifying the boundary layer diverter height for the HSCT nacelle installations. Boundary layer displacement thickness predictions together with CF calculations can be used to calculate the spillage and internal drag of wind tunnel flow though nacelles.

Local skin friction calculations corrected for local dynamic pressure effects can be used to estimate local surface temperatures.
The boundary layer thickness information presented in this paper will also provide some physical insight in to the fundamental features of turbulent flat plate flow.

COMPRESSIBLE FLOW FLAT PLATE SKIN FRICTION THEORY

The common theories for predicting compressible flow flat plate turbulent flow skin friction drag are all empirical in nature. The basis of any valid empirical theory is, first, it has to be based on good physical reasoning that attempts to simplify the representation of the flow phenomena by an approximate mathematical model. Secondly, it has to agree, of course, with appropriate test data within the scatter of that data. All of the theoretical flat plate formulations involve disposable constants that have been determined empirically. Thus, as is the rule for all empirical formulae, the theory should be, strictly speaking, only be applied where it has been justified by experiment. If there is a reasonable physical basis to the theory, then some extrapolation should be permissible.
This is equally true for current Navier Stokes CFD codes where viscous flow effects are determined using various turbulence models which approximate the local nature of the flow phenomena.

The common compressible turbulent flow skin friction theories assume that compressible turbulent skin friction drag could be obtained using well known incompressible skin friction equations by evaluating all of the fluid properties that appear in the incompressible equations at some appropriate reference temperature, T*. This assumption parallels the analytical transformation methods that had been used in laminar boundary compressible flow analyses. The assumption of an effective reference temperature in essence implies that the turbulent boundary shape and height are not strongly affected by Mach number. This will be further examined in this paper.
Experimentally, it is considered easier to obtain systematic force measurements of local skin friction drag then of average skin friction drag. Consequently, the initial step in the current evaluation process was to compare incompressible local skin friction data with the most generally accepted incompressible skin friction equations.

The most widely accepted equation for incompressible local skin friction, Cfi, is the Karmen-Schoenherr equation:

$$\frac{1}{\sqrt{Cfi}} = 4.15 * \log(Re\,x * Cfi) + 1.7 \qquad (1)$$

In this equation Rex is the Reynolds number based on the distance x, from the origin of the boundary layer.

A simpler to use but less sophisticated equation of incompressible skin friction is the modified Shultz-Grunow equation.

$$Cfi = 0.295 * (\mathrm{Log}\,(Re\ x))^{-2.45} \qquad (2)$$

The modification[1] was obtained by simply replacing the standard constant “0.288” by “0.295”. The modified constant was determined by statistical analyses to minimize the differences with the Karmen-Schoenherr equation and the Shultz-Grunow equation. The “mean” difference between the Cf values calculated by the Karmen-Schoenherr equation and by the modified Shultz-Grunow equation was found to be -0.0000031 over the complete Reynolds number range of 10^6 to 10^9. The standard deviation was calculated to be 0.00000452. Consequently, the simpler Shultz-Grunow equation was used in the current study.

In Figure 8, comparisons are made between measured incompressible local skin friction data from a number of sources[6,7,8,] with the modified Shultz-Grunow equation. The results of statistical analyses of the differences between the theory and the test data are also shown. The test data appears to scatter uniformly about the theoretical predictions for the entire Reynolds number range of the test data.
Statistical analysis of the differences between the test data and corresponding Cf predictions shows that the mean of the differences is ΔCf = -.000000671 which corresponds to an average difference of 0.13% .The standard deviation of data about the mean is approximately 0.7 counts of drag (ΔCf = 0.000067)

which corresponds to 2.8% of the corresponding predicted values.

The constant 0.288 in the original Shultz-Grunow equation would result in a mean difference between the test and theory of - 2.6% instead of 0.13% for the modified equation.

The modified Shultz-Grunow equation therefore appears to provide an accurate estimate of incompressible local skin friction coefficient over the entire range of Reynolds Numbers covered by the test data.

Using the Reference Temperature approach, the equation for compressible skin friction is then obtained by evaluating the fluid properties of density, ρ, and coefficient of viscosity, μ, at a reference temperature T*.

$$Cf = \frac{\rho^*}{\rho_\infty} Cfi = 0.295 \frac{\rho^*}{\rho_\infty} [\log(\mathrm{Re}\, x^*)]^{-2.45} \qquad (3)$$

The reference temperature Reynolds number, can be related to the free stream Reynolds number as:

$$\mathrm{Rex}^* = \mathrm{Rex} \frac{\rho^*}{\rho_\infty} \frac{\mu_\infty}{\mu^*} \qquad (4)$$

Assuming a perfect gas relation and that the pressure is constant across the boundary layer, the density varies inversely with the temperature. Therefore the compressible local skin friction equation becomes:

$$\mathrm{Cf} = 0.295 \frac{\mathrm{T}_\infty}{\mathrm{T}^*} \left[\log \left(\mathrm{Rex} \frac{\mathrm{T}_\infty}{\mathrm{T}^*} \frac{\mu_\infty}{\mu^*} \right) \right]^{-2.45} \qquad (5)$$

The various researchers have proposed numerous ideas for an appropriate reference temperature. These include:

- Use of the surface temperature ----this provided too large a compressibility correction
- Determined experimentally by specially designed experiments, --- Sommer / Short[10]
- Determine by correlation of Cf predictions with test data. --- Spaulding / Chi[11]
- Velocity averaged enthalpy across a boundary layer ---- Monoghan[12]
- Semi-analytic formulations -- Van Driest (Ref 2)

In the current study the reference temperatures selected for evaluation included: the Monagham mean enthalpy equation, and the Sommer / Short equation. Previous studies have shown both to provide accurate assessments of compressible skin friction.

For adiabatic wall conditions, the reference temperature is related to the free stream Mach number, M_∞, As:

$$\frac{T^*}{T_\infty} = 1 + Kr \bullet r(\sigma - 1) M_\infty^2 \qquad (6)$$

where:

- Kr is a constant that depends on the particular T* method
- r = boundary Layer Recovery factor ~0.89
- σ = Ratio of specific heats = 1.4

Figure 9 shows some of the compressible flow skin friction data used to validate the flat plate theories. This compares the compressible skin friction predictions obtained using two commonly used T* methods, the Monaghan T* and the Sommer-Short T* method.

The Sommer-Short T* equation results in compressible skin friction values slightly but consistently higher than predicted using the Monaghan method.

Statistical analyses were made of the differences between Cf predictions and the corresponding test data as shown in figure 10. The theoretical predictions were obtained using three different T* equations. The "scatter" in the test - theory increments are essentially equal. The mean of the differences between the test and theory, however differs between the predictions obtained using the different T* equations.

The "mean" of the theory - test differences obtained using the Monaghan T* equation is approximately 1% low. The "mean" of the theory - test differences obtained using the Sommer-Short T* equation is approximately 1% high. The constant for the Kulfan T* equation was therefore chosen to be the average of the Sommer-Short and the Monaghan constants.

This essentially resulted in a mean error between the test data and the theoretical predictions of zero.

The test data scatter about the mean has a standard deviation of about 4.5%. This large scatter is in part due to the variations of Reynolds number of the test data. The Reynolds number for the test data 10^6 to 10^7. The theoretical calculations were made for a Reynolds number of 5×10^6

Figure 11 shows comparisons of predicted skin friction with test data for 3 different supersonic Mach numbers. The T* equations can also be used to convert the compressible skin friction to equivalent incompressible data. This approach can provide a convenient means to assess the accuracy of the theoretical methods to account for compressibility effects simultaneously over a range of Mach numbers and Reynolds numbers

This transformation procedure, as shown in Figure 12, "collapses" all of the test data about the incompressible skin friction curve. The transformed experimental data consists of six different sets of test data obtained at Mach numbers from 1.7 to 2.95. The incompressible Mach number data from figure 11 have not been included in the above figure since it was desired to independently assess the ability of the different T* equations to account for Mach number effects on skin friction. The figure also includes the statistically determined differences between the transformed equivalent incompressible skin friction data and the modified Shultz-Grunow theoretical Cf predictions. The Kulfan T* equation was used for the transformation process. The "mean" of the differences between the transformed skin friction data and the incompressible Cf predictions is essentially zero.

The " scatter" of the test has a standard deviation of about 1 drag count ($\Delta Cf \sim 0.0001$). This corresponds to about a 3.8% scatter of the test data about the theoretical Cf predictions over the entire Reynolds number range and Mach number conditions represented by the test data.

On the average, the Monaghan predictions were found to underestimate the corresponding test data by about 0.3 counts or 1.2 % and the Sommer-Short predictions were about 0.3 counts higher corresponding to about 1.0%. The Kulfan T* method appears to provide the best estimate of the compressibility effects for the flat plate turbulent flow skin friction.

The "scatter" in the difference between compressible theoretical - experimental transformed skin friction data are slightly higher than the corresponding scatter in the incompressible data shown in figure 8. (3.8% versus 2.7%).

The selected T* equation was then applied to the calculation of compressible average skin friction.

The most widely accepted in compressible average skin friction equation is the Karmen-Schoenherr equation:

$$\frac{0.242}{\sqrt{CFi}} = \log(Rex \cdot CFi) \qquad (7)$$

Comparisons were made calculations using the Karmen-Schoenherr equation with the less sophisticated modified Prandtl-Schlichting equation.

$$CFi = 0.463 * \left[\log(Re\ x)\right]^{-2.6} \qquad (8)$$

The modification was simply replacing the standard constant "0.460" by "0.463". The mean difference between the CF values calculated by the Prandtl-Schlichting equation and by the Karmen-Schoenherr equation was -0.0000013 over the complete Reynolds number range. The standard deviation was calculated to be 0.00000678. Consequently, the simpler modified Prandtl-Schlichting equation was used in the current study.

It is interesting that though out their technical careers. Prandtl and Von Karmen often tackled the same fluid dynamic problem. Their results almost always differed in the analytical formulations and the form of the equations describing the flow phenomena. Computed results were always within a few percent of each other.

Comparisons between theoretical and experimental average skin friction data are shown in Figure 13. The lack of additional test data is attributed to the difficulty in obtaining average skin friction data by direct force measurements. Often, average skin friction data are obtained by application of the momentum integral equation to boundary layer velocity profile measurements. The uncertainties of the interference between the pitot probes used for the measurements and the surface introduces errors that are difficult to correct. The data shown for Mach 2.0 and Mach 2.5, were obtained from force measurements on the cylindrical portion of a cone-cylindrical body of revolution. The Mach 1.61 data were obtained with an ogive - cylinder body of revolution. Three-dimensional effects are considered to be small on the cylindrical sections. However determining the "effective origin" for the flow over the cylindrical can certainly introduce substantial errors. At supersonic speeds it was also necessary to

remove the wave drag on the nose of the model from the test data.

The theoretical predictions match the Mach 2.0 and Mach 2.5 data quite well. Theory under estimated the friction drag at Mach 1.6. This is believed to be due to a bias in the test data.

The results of the data correlation shown in this paper indicate that comparisons with local skin friction data is the best approach to evaluate methods for prediction of flat plate skin friction drag.

TURBULENT FLOW FLAT PLATE BOUNDARY LAYER GROWTH

During the course of the previous investigation[3], experimental measurements of velocity profiles were found. It was also then possible to study the growth characteristics of a turbulent boundary layer over a flat plate. A method was developed to predict the growth of a turbulent boundary layer on a flat plate. This method has been revised in the current study.

The edge of a turbulent boundary layer bounded by a free stream of negligible turbulence has a sharp but very irregular outer limit. The velocity tends to approach the free stream velocity asymptotically. Hence the definition of the thickness of a turbulent boundary layer is subject to many variations. A common definition of the edge of the boundary layer, δ, is the height at which the velocity is equal to some percentage of the free stream value. Typically a value of 0.995 is used.

Because of the asymptotic nature of a turbulent boundary layer, other parameters are often used to characterize the boundary layer growth. These include the displacement thickness, δ^*, the momentum thickness, θ, and the shape factor H.

The displacement thickness is defined as :

$$\delta^* = \int_0^\infty \left[1 - \frac{\rho}{\rho_\infty} \frac{u}{U_\infty} \right] dy \qquad (9)$$

The displacement thickness defines the amount that the flow streamlines diverge around the surface because of the boundary layer flow. Calculations of the displacement thickness are often used in the estimation of the spillage characteristics and the internal drag of flow-through nacelles on wind tunnel models.

The momentum thickness is defined as :

$$\theta = \int_0^\infty \frac{\rho}{\rho_\infty} \frac{u}{U_\infty} \left[1 - \frac{u}{U_\infty} \right] dy \qquad (10)$$

The momentum thickness defines a height of free stream flow that contains the same momentum as lost across the boundary layer at any specified streamwise station.

The momentum thickness on a flat plate is directly related to the average skin friction coefficient as:

$$\theta = (X\ CF)/2 \qquad (11)$$

One technique used to determine average skin friction on a flat plate is to measure the velocity profile, and then integrate the experimental velocity profile to obtain the momentum thickness. Then the average skin friction coefficient is calculated using the above equation. Using this procedure it is generally very difficult to obtain consistent and accurate assessments of the friction drag.

The boundary layer shape factor is defined as

$$H = \delta^* / \theta \qquad (12)$$

The shape factor, H, is often used to predict the separation tendency of a boundary layer with an adverse pressure gradient.

In incompressible flow, the value of Hi for a flat plate turbulent flow is a unique function of the "shape" of the boundary layer. Clauser[13] developed an equation for H based on a more sophisticated representation of the boundary layer based on the "velocity defect" concept. Experimental values of the incompressible shape factor, Hi, are compared with a modified version of Clauser's equation in figure 14. In this modified equation, the constant 4.75 replaced Clauser's original value of 4.31.

The modified version of Clauser's equation is:

$$Hi = \frac{1}{1 - 4.75 * \sqrt{Cfi}} \qquad (13)$$

Also shown in the figure 14 are numerical values for Hi calculated by Cole[17] using "log" wall relations for the boundary layer. The modified Clauser equation is seen to match very with Cole's results and with the test data.

Monaghan[12] Showed that the turbulent boundary layer shape factor, H, for compressible flow can be obtained from the incompressible shape factor by multiply the incompressible shape factor by a compressibility correction factor, H/Hi, that depends on the free stream temperature T_{∞}, the wall temperature T_w, and the recovery temperature T_r, by the equation:

$$\frac{H}{Hi} = 1 + \left(\frac{T_w}{T_\infty} - 1\right) + \left(\frac{T_r}{T_\infty} - 1\right) \qquad (14)$$

For an insulated surface this equation becomes:

$$\frac{H}{Hi} = 1 + r(\gamma - 1)M_\infty^2 \qquad (15)$$

Experimental compressible data also shown figure 14 appears to validate this equation. Hence, the shape factor for fully turbulent flat plate flow can be can be calculated as the product of two terms. One term depends only on Reynolds number and the second term depends only on Mach number. The equation implies that boundary layer displacement effects become much larger than the momentum thickness as Mach number increases.

TURBULENT FLOW FLAT PLATE BOUNDARY LAYER VELOCITY PROFILE

Often in boundary layer studies, it is convenient to represent the velocity profile by a power law relation of the form:

$$\frac{u}{U_\infty} = \left(\frac{y}{\delta}\right)^{\frac{1}{N}} \qquad (16)$$

- y = distance in the boundary layer normal to the surface
- u = the local streamwise velocity in the boundary layer.
- U_∞ = freestream velocity

The disposable constant, N, for the empirical equation has been determined from correlations of a large number of measured velocity profiles from six independent sources [4,6,7,14,27,28].

Figure 15 contains a typical plot of experimental profile measurements on a conventional scale and on a logarithmic scale. The data in the logarithmic plot shows the approximate velocity profile representation. The regions of the boundary layer near the surface and near the upper portion can each be represented by a distinct straight line. This is indeed as it should be, since a more accurate description of a turbulent boundary layer requires the use of two functions. These include the "law of the Wall" which applies near the surface and the "Law of the Wake" which applies to the intermediate/outer portion of the boundary layer[13]. The velocity profile exponent "N" corresponds to the slope of the mean line shown in the figure. The corresponding value of the boundary layer thickness, δ, is defined as the height where the mean line intersects the value of $u/U_\infty = 1.0$

Incompressible velocity profile data from a number of independent sources were used to determine "appropriate" values of N to represent a turbulent boundary layer. The results as shown in Figure 16, indicate that the value of "N" is strongly dependent on Reynolds number. An analytical equation was developed to represent the experimental data for the velocity factor.

$$N = \max\left[\frac{0.1035 - 2*(Cfi)^{0.75}}{(Cfi)^{0.75}}, 6.0\right] \qquad (14)$$

This equation is also shown in the figure.

Values of "N" determined from compressible boundary layer measurements for a number of Mach numbers from 1.5 to 4.2 are also shown. The compressible values of "N" appear to reasonably scatter about the empirical equation that was developed from the incompressible velocity profile data. Thus it appears that the shape of a turbulent depends primarily on Reynolds number but is relatively independent of Mach number. This result should not be surprising for it is implied by the concept of the reference temperature approach to calculate supersonic skin friction drag. Skin friction in general, depends on the shape of the boundary layer as well as the density and viscosity in the boundary. The reference temperature method as defined earlier in this note assumes that compressibility

effects on flat plate flow, only changes the effective values of density and viscosity. Hence, Mach number would not significantly change the velocity profile shape.

The various boundary layer growth characteristics were calculated from the typical measured velocity profile data shown in Figure 15, and also using the approximate "power law" velocity profile. The results are summarized in the table below

	Measured Profile	Approximate Profile	"Error" %
δ*	0.0803	0.0801	-0.25
θ	0.0592	0.0613	3.5
H	1.357	1.307	-3.7

The approximate velocity profile does provides a good approximation to the turbulent boundary layer growth characteristics. This is particularly true for the displacement thickness since the velocity profile fit process essentially minimizes the difference between the measured velocity and the velocity corresponding to the approximate boundary layer profile. This in turn minimizes the displacement thickness error.

TURBULENT FLOW FLAT PLATE BOUNDARY LAYER GROWTH

The approximate form of the turbulent boundary velocity profile has been used to develop a method for predicting the flat plate turbulent flow boundary layer thickness. The boundary layer thickness is defined as the height at which the velocity is essentially equal to the free stream velocity.

The boundary layer thickness can be related to the displacement thickness by using the approximate velocity profile in the integral equation for the displacement thickness as:

$$\frac{\delta^*}{\delta} = \int_0^1 \left[1 - \frac{\rho}{\rho_\infty} \left(\frac{y}{\delta} \right)^{\frac{1}{N}} d\frac{y}{\delta} \right] \qquad (15)$$

And

$$\delta = \frac{\delta^*}{\left(\frac{\delta^*}{\delta} \right)} \qquad (16)$$

The displacement thickness can be obtained from equations 11, 13 and 15 as:

$$\delta^* = \theta * H_i * \left(\frac{H}{H_i} \right) \qquad (17)$$

Calculations of the variation of incompressible flat plate boundary layer thickness are compared with test data in figure 17. The theoretical predictions appear to closely match the test data. Comparisons of compressible boundary layer thickness predictions are also compared with test data in this figure for Mach numbers of 1.7, 2.0 and 3.0. Although there is quite a bit of data scatter, the data appears to validate the boundary layer thickness predictions.

These results appear to substantiate the conclusion that the thickness of a turbulent boundary layer is indeed relatively insensitive to Mach number.

Boundary layer thickness and displacement thickness have been calculated for a range of Reynolds numbers and Mach numbers from 0 to 3 using the methods presented in this paper. The results are shown in figure 18. The overall boundary layer thickness is seen to be relatively insensitive to Mach number. The boundary layer displacement thickness, however, grows rapidly as Mach number increases.

BOEING PHANTOM WORKS, LONG BEACH, BPW-LB CFD VISCOUS DRAG ANALYSES

The BPW-LB fully turbulent flat plate average skin friction predictions were made using the Navier-Stokes Code, CFL3D[18] and a number of turbulence models. The turbulence models used in the calculations are representative of turbulence model categories[19,20] ranging from most simple to most sophisticated and include:

- "zero-equation" (algebraic) model - Baldwin-Lomax[21,22]
- "one-equation" model - Spalart- Allmaras[23]
- "two-equation" model - Menter's SST[24,25]

The computational grids were defined to be uniform in the main flow direction to avoid a singularity at leading

edge of flat plate. Exponential stretching were applied to the grids in direction normal to wall within boundary layer to provide the accurate resolution requirement with the memory constraints. Uniform grid spacing in normal direction was used outside boundary layer to minimize the effect of truncation error on the solutions. Four sets of grids were used in the computational process. These included 17x25 (axial by normal) nodes; 33x49 nodes; 65x97 nodes and 129x193 nodes. The finest grid was the baseline grid. The coarser grids were generated by sequentially skipping every other node.
Convergence acceleration techniques that were employed included grid sequencing, multigrid and local time stepping. The computations were carried out on workstations using 32-bit arithmetic. The residuals were overall converged by 5 orders of magnitude. The finest grid solutions converged by about two orders of magnitude due to machine accuracy limitations.

Skin friction calculations were based on Richardson extrapolation process. Skin friction values were plotted against the inverse of the grid resolution (=1/number of nodes). Linear convergence indicated the second-order spatial accuracy. Asymptotic skin friction values were obtained from linear extrapolation to infinitely fine grids. The skin friction calculations were obtained for Mach numbers of 0.5, 1.5, 2.25 and 2.5. The results of the calculations are presented for a range of Reynolds numbers from 10^6 to $200x10^6$.

Comparisons of average skin friction predictions obtained using the Baldwin-Lomax turbulence model, with the flat plate calculations are shown in Figure 19. The Reynolds numbers for typical wind tunnel conditions and for typical full scale or flight conditions are indicated in the figure.
Following the transformation procedure shown in Figure 11, the CFD computed skin friction values were converted to equivalent incompressible values. The results are shown in Figure 20. A “mean” level of all the transformed calculations is also shown. The results indicate that the calculations with the Baldwin-Lomax turbulence model appears to match the Reynolds number trends of the flat plate theory. The CFD calculations also are shown as a ratio to the flat plate theory incompressible values in figure 20. The Mach trend of the CFD calculations does not match the flat plate theory too well. \
The differences between the CFL3D predictions and the flat plate theory are shown in figure 21 both as drag increments and as percentage differences. The differences in the predictions are seen to be both Reynolds number and Mach number dependent. The absolute differences between CFD calculations of CF and the corresponding flat plate values over the range of wind tunnel to flight are essentially within plus and minus 1 friction count (0.0001). This might be construed as an excellent agreement. However one count of skin friction drag corresponds to nearly 3.5 counts of airplane drag since the wetted area ratio for a typical HSCT is on the order of 3.5. On a percentage basis, the differences are seen to be significant. The CFD predictions at wind tunnel Reynolds numbers vary from 4% low at Mach 0.5 to 3% high at Mach 2.5 relative to the flat plate theory and hence also to the mean of the experimental data base.

The values of CF, calculated using the Spalart-Allmaras turbulence model, are compared with the corresponding flat plate theory values in figure 22. The CFD predictions of CF are seem to be significantly less then the flat plate theory at the lowest Reynolds numbers.

The CFD results are also shown in figure 23 as equivalent incompressible values, and as ratios to the flat plate incompressible drag levels. The Reynolds number trend of the Spalart-Allmaras calculations differs quite a bit from the incompressible flat plate values. The Mach number trend also differs from the flat plate theory.
The differences between the CFD calculations and the corresponding flat plate values are shown in figure 24. At the incremental differences, again may appear to be small. However at wind tunnel Reynolds, the CFD predictions at Mach 0.5 are 4% low and at the highest Mach number are 3% high. The CFD predictions vary from 3% high to 7% high as the Mach number is increased at typical Flight Reynolds Numbers.
Later in this paper it will be shown that the Spalart-Allmaras CF predictions have a laminar flow type of friction drag characteristics at the lowest Reynolds numbers. This is then followed by a transitional type flow friction drag rise and finally turbulent flow at the

higher Reynolds numbers. This accounts for the reduced levels of friction drag at the lowest Reynolds numbers.

CF calculations made by BPW-LB were also obtained using the Menter's SST turbulence model. The results are compared with the flat plate predictions in figure 25.
The results are shown in figure 26 as equivalent Cfe values and as ratios to the incompressible flat plate values. The calculations with Menter's SST turbulence model match the Reynolds trend quite well but tend to miss the Mach number trend as did the calculations with the other turbulence models.

The differences between the CFD and the flat plate calculations are shown in Figure 27. The CFD results are approximately 1 count low (-0.0001) to 0.5 count high for all of the calculations above typical wind tunnel test Reynolds number. The differences between CFD and the flat plate theory are less then with the other two turbulence models.

The previous comparisons of the CFL3D with the flat plate theory are summarized in figure 28, but with the very low Reynolds number results removed since this is below the region of interest for practical applications. It is seen that the predictions obtained with all of the turbulence models at wind tunnel Reynolds numbers are quite consistent in the Mach number trends and levels. At Flight Reynolds numbers the Baldwin - Lomax and the Menter's SST results are nearly the same. The Spalart-Allmaras predictions are a few percent higher then the results obtained using the other turbulence models.

NASA AMES RESEARCH CENTER CFD VISCOUS DRAG ANALYSES

The fully turbulent flow flat plate skin friction calculations made by NASA Ames were obtained using the OVERFLOW code v1.8f. Two turbulence models were evaluated: the Spalart-Allmaras one-equation model and Menter's 2-equations SST model.
The grid contained 120 points in the streamwise and wall-normal directions. The grid in the wall-normal direction was clustered at the wall such that y+ at the first point off the surface had values between 0.02 and 0.15 depending on Mach and local Reynolds numbers. Wall-normal points were evenly spaced for the first 4 points off the surface and stretched from the fifth point to the outer boundary. This type of grid definition is needed to obtain high-fidelity skin friction predictions from OVERFLOW. The wall spacing is considered a little finer than needed, especially at the higher Mach numbers. Experience with numerous other calculations (primarily at Mach 2.4) using various grids provided a sense of confidence in the validity of the results.
Solutions were computed at 5 Mach numbers (0.5, 0.9, 1.5, 2.0, and 2.4) at a length Reynolds number of 6 million. At Mach 2.4 additional calculations were made at full scale Reynolds number of 200 million.

Figure 29 shows a comparison of the local skin friction calculations using the Spalart-Allmaras turbulence model versus the corresponding flat plate theory calculations. At the low Reynolds numbers, as a result of what appears to be pseudo laminar / transitional flow calculations within the Spalart-Allmaras turbulence model, the CFD predictions fall below the flat plate theory. The CFD predictions then appear to attempt to overshoot the fully turbulent flow level as would be the case for partially laminar flow. At the highest Reynolds Numbers, local skin friction CFD calculations are slightly less than the flat plate values at low Mach numbers. At the higher Mach numbers, CFD predictions tended to exceed the flat plate theory values.
The differences between the CFD and the flat plate predictions of local skin friction drag are also shown as a percentage difference relative to the flat plate theory. At wind tunnel Reynolds numbers (approximately 6 x 10^6), the CFD predictions differ from the flat plate theory by approximately minus 1 to plus 3.4% as the Mach Number increases from 0.5 to 2.4.

The NASA Ames average skin friction calculations, obtained with the Spalart-Allmaras turbulence model, are compared with the with the flat plate theory in figure 30. Similar to the local skin friction results, the CFD average CF predictions are significantly less then the flat plate theory at the lowest Reynolds numbers and tend to match better at wind tunnel Reynolds numbers. At the lowest Reynolds numbers, the CFD predictions are significantly less then the flat plate

theory. However, near wind tunnel Reynolds the CFD predictions are within plus and minus 2 %.

The local skin friction drags calculated using the Menter's SST turbulence model are compared with the flat theory in figure 31. The results obtained using the Menter's SST Turbulence model do not show the same pseudo laminar flow effects as the predictions obtained with the Spalart-Allmaras turbulence model. However the CFD predictions all fall below the flat plate theory. The differences between the CFD and flat plate predictions are also shown in percent relative to the flat plate theory. The CFD predictions are significantly less then the flat plate theory at the lower Reynolds numbers .The CFD predictions vary from –9% to –3% relative to the flat plate theory over the Reynolds number range.

The NASA Ames average skin friction calculations, obtained with Menter's SST turbulence model, are compared with the flat plate theory results in figure 32. Similar to the local skin friction results, the CFD average CF predictions are significantly less then the flat plate theory at the lowest Mach numbers and tend to match the flat plate theory better at the highest Mach number (2.4).

The initial set of skin friction calculations by NASA Ames, were obtained for an overall length Reynolds number of about 6.6 million. Calculations were also made at Mach 2.4 for overall length Reynolds number of 200 million corresponding to full-scale conditions. The full-scale calculations are compared with the wind tunnel results in figure 33. The local skin friction for the wind tunnel analysis converges quite well into the flight condition results. The CFD predictions vary from 3% high at wind tunnel conditions to 5% at full-scale conditions relative to the flat plate theory.

The full-scale CFD average skin friction calculations using the Spalart-Allmaras turbulence are shown in figure 34. The differences between the CFD average skin friction calculations and the flat plate theory calculations are seen to be very Reynolds number dependent and vary from 3% to nearly 8% high over the range of wind tunnel to flight conditions.

The corresponding results obtained with Menter's SST turbulent model are shown in figures 35 and 36. The Local skin friction CFD predictions are significantly vary with from –2% to plus 2% over the Reynolds range of interest. The average skin friction predictions vary from 1% to 3.5% higher then the flat plate theory over the Reynolds Number range of interest.

The results of the NASA Ames CFD calculations are summarized in figure 37 as ratios to the corresponding flat plate theory incompressible values. The Spalart-Allmaras calculations match the flat plate theory trend quire well. The Mach number trend with the Menter's SST turbulence model differs significantly from the flat plate theory.

BOEING COMMERCIAL AIRPLANES, SEATTLE, BCAG CFD VISCOUS DRAG ANALYSES

The flat plate skin friction calculations by Boeing Commercial Airplane Group in Seattle (BCAG), were also obtained with the OVERFLOW code using a number of different turbulence models. The effect of different vertical grid spacing techniques were also examined. The standard vertical grid spacing was similar to that used by NASA Ames and was uniformly spaced near the surface. Both local and average skin friction values were calculated at Mach 0.9 and 2.4 for a typical wind tunnel Reynolds number and a typical flight Reynolds number. Local skin friction was calculated for different locations on the flat plate. Integration of the local skin friction results then gave predictions of average skin friction for a wide range of Reynolds numbers based on the distance back of the leading edge of the flat plate.

The OVERFLOW local skin friction and average skin friction calculations made using the Baldwin-Lomax turbulence model are compared with the flat plate theory in figures 38 and 39 respectively. The overflow predictions are seen to be significantly less then the flat plate theory.

The local skin friction calculated with the Spalart-Allmaras turbulence model is compared with the flat plate theory in this figure 40. At Mach 0.9, the CFD predictions vary from - 2 % to +1% of the flat plate

theory over the wind tunnel to flight Reynolds number range. At Mach 2.4, the CFD predictions are from 4% to 5.5% higher then the flat plate predictions.

The corresponding differences between the CFD predictions of the average skin friction obtained with the Spalart-Allmaras turbulence model and the flat plate theory vary significantly with Reynolds number as shown in figure 41. The CFD predictions at the lowest Reynolds numbers fall far below the flat plate theory. This is most likely due to the pseudo transitional flow characteristic that is inherent in the Spalart - Allmaras turbulence model. The Mach = 0.9 predictions relative to the flat plate theory, vary from -4% at wind tunnel Reynolds numbers to +1.5% at full scale. The Mach 2.4 predictions vary from 1% to 6% higher then the flat plate theory.

The results obtained with the Menter's turbulence model also indicate that the CFD predicts different Mach number and Reynolds numbers trends then the flat plate theory as shown in figures 42 and 43. The CFD predictions of local skin friction is far below the flat plate theory for Mach 0.9. The Mach 2.4 predictions are within -1% to +2% of the flat plate theory over the wind tunnel to the flight range of Reynolds numbers. The average skin friction results are quite similar to the local skin friction results. Over the range of Reynolds from wind tunnel to flight, the CFD predictions at Mach 0.9 are 7 % to 3% lower then the flat plate theory. The Mach 2.4 predictions for the same range of Reynolds numbers vary from - 2% to +2% of the flat plate values.

The percentage errors in all of the BCAG OVERFLOW calculations are summarized in figure 44 with the very low Reynolds number results removed. The height of each data bar indicates the variation in the OVERFLOW predicted Reynolds number trends as compared to the flat plate predictions.

The Baldwin-Lomax predictions are consistently less then the flat plate theory. The Spalart-Allmaras calculations agree the best with the flat plate theory at wind tunnel Reynolds numbers. The Menter calculations are the closest to the flat plate predictions at Mach 2.4 of all the turbulence models.

The BCAG OVERFLOW results presented thus far were all calculated using a constant vertical grid spacing close to the surface of the flat plate. Results obtained using a common stretched grid vertical spacing are compared with the constant grid spacing result in figure 45. The CFD predictions are seen to be very dependent on the vertical grid spacing scheme. The constant grid spacing predictions tend to agree better with the flat plate theory then the stretched grid spacing predictions. This confirmed the results of earlier studies.

OVERALL ASSESSMENT ON THE CFD VISCOUS DRAG PREDICTIONS

Figure 46 contains a comparative summary of all of the CFD average skin friction predictions relative to the flat plate theory and hence to the mean of the experimental flat plate. The comparisons shown are for Mach 0.5 or 0.9 and Mach 2.4 or 2.5. The four sets of calculations include:

- BPW-LB CFL3D results (L)
- BCAG OVERFLOW results with two different vertical grid schemes (S1 and S2)
- NASA Ames OVERFLOW results. (A)

Both wind tunnel and flight predictions are shown for the BPW-LB and the BCAG results.

The NASA Ames results include only wind tunnel predictions for M = 0.9, and both wind tunnel and flight predictions for Mach 2.4

It is apparent that the BCAG stretched grid results (S1) do not agree as well as the uniform grid calculations (S2). The Spalart-Allmaras results are quite consistent for all three organizations (L, S2 and A). The Spalart-Allmaras seem to provide the best agreement with the flat plate theory at Mach 0.9 even though the Reynolds Numbers trends differ. The Menters SST predictions seem to match the flat plate theory the best at Mach 2.4. The scatter band for the test data relative to the flat plate theory is also shown in the figure. It us seen that the variations in the CFD predictions far exceeds the scatter of the test data.

Viscous drag predictions for a commercial aircraft are typically used in three common applications

- Prediction of the drag of a scale model at wind tunnel conditions

- Prediction of the drag of an airplane at full-scale conditions
- Extrapolation of wind tunnel results to full-scale conditions

In order to understand the potential impact of the uncertainties in the viscous drag predictions, the differences between the CFD predictions and the flat plate theory have been converted into airplane drag counts. The equivalent drag counts are obtained by multiplying the average skin friction increments by the wetted area ratio, Awet/Sref, for a typical HSCT type configuration:

$$\Delta CDF = [CF_{CFD} - CF_{FP}]\frac{Awet}{Sref} \qquad (17)$$

where: $\frac{Awet}{Sref} \approx 3.5$

Where:

- CF_{CFD} = The average skin friction computed by the
- CFD code
- CF_{FP} = The flat plate theory skin friction which represents the mean of the experimental database
- Awet = Overall wetted area of the aircraft configuration
- Sref = Wing reference area

The impact of the prediction differences on the drag at wind tunnel conditions is shown in Figure 47. The average error of the predictions at subsonic conditions is about 3.5 drag counts low. The predictions actually vary from –2.8 to –6.0 drag counts too low. At the supersonic conditions the average error of the predictions is about ½ drag count high. The predictions vary from plus to minus 2 drag counts relative to the flat plate theory.

The full-scale prediction errors are shown in figure 48. At the subsonic condition, the average error of all predictions is about 1 drag count low and the range of errors varies from – 2.6 to +1.5 drag counts. The average error at Mach 2.4 is +1.66 drag counts with a range of errors from –0.7 to +3.1 drag counts. As shown in the Introduction Section, a one count drag error, (ΔCD ~ 0.0001) is equivalent to a structural weight error of about 2,000lbs and would impact the overall gross weight by nearly 10,000lbs. Hence, the impact of the uncertainties in the existing CFD predictions of the friction drag, are indeed very significant.

The full-scale drag levels can also be obtained by using the CFD predictions of the viscous drag to extrapolate wind tunnel data to the full-scale conditions. The full-scale predictions are then achieved by adding the difference between the full-scale and the corresponding wind tunnel viscous drag predictions to the wind tunnel data. The errors in the wind tunnel to full-scale corrections are shown in figure 49. The average drag error at Mach = 0.9 is +3.5 drag counts with a error range of +0.7 to 409 drag counts. This extrapolation process in this instance resulted in a greater error then using the direct calculation of the friction drag at full scale conditions. At Mach 2.4 the average error is about 1 ¼ drag counts with a range of -0.5 to + 2 drag counts. This is just slightly better then the direct calculation of the full-scale drag.

SUMMARY

For the study presented in this paper, local skin friction measurement data from a number of independent different sources were selected as the basis for evaluation of the CFD predictions. The test data appeared to exhibit a rather significant scatter in the data across the range of Reynolds numbers and Mach numbers covered by the test data. The “mean” of the test data was accurately represented by a modified flat plate skin friction theory. The flat plate theory was subsequently assumed to be the “correct” values for comparison with the CFD predictions.

The theoretical predictions by each organization represented what were considered to be accurate representations of the flow physics over a flat plate using the grid definition techniques and concepts consistent with their HSCT design and analysis studies. At least one turbulence model, the Spalart-Allmaras model, had difficulty in simulating fully turbulent flow from the leading edge of the plate. The condition of fully turbulent flow, however, is a condition that really does not exist in nature either.

It is obvious, that even with an apparently simple test case, significant differences exist between friction drag

predictions obtained by different organizations, using different CFD codes and various turbulence models. The predictions differed from the test database in magnitude and also in both the Mach number trend and the Reynolds numbers trend. The variations between the CFD predictions and the mean values of the test data was substantially greater then the scatter of the experimental measurements. The differences when considered as absolute skin friction counts may appear small. But when interpreted airplane drag counts, the differences are seen to be significant. This places the requirement for a high degree of accuracy on both the test database and any CFD calculations.

This apparently simple test case of a flat plate with fully turbulent flow is however difficult to simulate both experimentally and analytically. The experimental test measurement processes to measure either local skin friction are difficult to conduct and difficult to obtain consistent quality measurements. The condition of fully turbulent must be simulated by the use of boundary layer trips and the data must be further corrected to an equivalent "naturally" fully turbulent flow condition. Analytical difficulty occurs not only in determining an "appropriate" grid technique and selection of an appropriate turbulence model. In some instances, representation of a fully turbulent flow condition is inconsistent with the nature of the turbulence model.

The results have identified the magnitude of the uncertainty that can exist with any of the predictions Further activities should be conducted to resolve the differences between the various predictions and the test database. These activities should include:

- Selection and definition of appropriate CFD validation geometries that may or may not include a flat plate plus other geometry concepts.
- Generation of the appropriate test database from existing test data and from specifically designed experimental programs.
- Selection of the measurement techniques and definition of the necessary data corrections
- Selection of a restricted set of evaluation CFD codes and possible turbulence models.
- Definition of consistent and appropriate grid definitions and convergence schemes.
- Assessments of the predictions and possible refinement of the analysis codes and techniques.
- Determine if the analysis processes and techniques determined in the evaluation studies are also appropriate for more sophisticated geometries.
- This process may require of a multi-phase program with a variety of configurations and wind tunnel test programs in a variety of test facilities.

CONCLUSIONS

- Existing Database Has Rather Large Range of Data Scatter ~ plus to minus 3.8%
- Modified Incompressible Equations and Improved T*/T Method Predict the "Mean" of Available Flat Plate Skin Friction Drag Measurements
- Need Additional / Quality Experimental CF Data:
  - Average and local Skin Friction
  - Locate Available Existing Data
  - Additional Test Programs
  - Symmetric Model Tests
  - Segmented Axi-symmetric Body of Revolution
  - New / Improved Measurement techniques
  - High Reynolds Number Data
- Range of Variation in CFD Predictions (~ -7 % to +14%) Significantly Greater then Test Database Data Scatter
- CFD Predictions Relative to Flat Plate Theory Differ in Both Reynolds Number and Mach Number Trends
- Magnitude of Analyses Uncertainties ~ Major Impact on HSCT Design Assessment
  ΔTOGW ~ -7,000 to + 31,000 lbs
  ΔOEW ~ -1,400 to + 6,200 lbs
- Need "Second Series" of CFD Predictions of Flat Plate Skin Friction Drag Assessments
  - Is the "Flat Plate" a Meaningful Evaluation Configuration ?
  - Selection of Codes and Analyses Techniques Based on Original Study Results
  - Joint Agreement on Evaluation Data
  - Definition of Evaluation Conditions
- Proceed as in Original "Plan" to More Sophisticated Geometries

REFERENCES

1. Kulfan, R. M.., “Historic Background on Flat Plate Turbulent Flow Skin Friction and Boundary Layer Growth.”, 1998 NASA High-Speed Research Program Aerodynamic Performance Workshop, Vol. 1, Part 1 Page: 477-513, Dec 01, 1999, NASA/CP-1999-209692/Vol. 1/Pt. 1
2. Kulfan, R. M., “Assessment of CFD Predictions of Flat Plate Skin Friction”, 1999 NASA High-Speed Research Program Aerodynamic Performance Workshop, Vol. 1, Part 1 Page: 253-300, Dec 01, 1999, NASA/CP-1999-209704/Vol. 1/pt. 1
3. Kulfan, R. M., "Turbulent Boundary Layer Flow Past a Smooth Adiabatic Flat Plate", Boeing Document D6-7161, May 1961
4. Shutts, W. H., Hartwig, W. H., and Weiler, J. E. "Final Report on Turbulent Boundary Layer and Skin Friction Measurements on a Smooth, Thermally Insulated Flat Plate at Supersonic Speeds." Defense Research Laboratory Report. D.R.L. - 364, C.M. - 823.
5. Dhawan, S. "Direct Measurements of Skin Friction." NACA Report 1121, 1953.
6. Smith, D. W., and Walker, J. H. "Skin Friction Measurements in Incompressible Flow." NACA TN 4231, 1958.
7. Matting, F. W., Chapman, D. R., Nyholm, J. R., Thomas, A. G. "Turbulent Skin Friction at High Mach Numbers and Reynolds Numbers in Air and Helium." NASA R-82.
8. Matting, F. We, Chapman, D. R., Nyholm, J. R., Thomas, A. G. "Turbulent Skin Friction at High Mach Numbers and Reynolds Numbers." PROCEEDINGS OF THE 1959 HEAT TRANSFER AND FLUID MECHANICS INSTITUTE. Stanford University Press, 1959.
9. Smith, D. W., and Walker, J. H. "Skin Friction Measurements in Incompressible Flow." NACA TR R-26, 1959.
10. Sommer, S. C., and Short, B. J. "Free Flight Measurements of Skin Friction of Turbulent Boundary Layer Skin Friction in the Presence of Severe Aerodynamic Heating at Mach Numbers from 2.8 to 7.0." NACA TN 3391, March 1955
11. White, F. M. VISCOUS FLUID FLOW, Mc Graw - Hill Book Company, 1974
12. Monaghan, R. J. "On the Behavior of Boundary Layers at Supersonic Speeds." I.A.S. – RAS Proceedings, 1955
13. Lin, C. C. TURBULENT FLOWS AND HEAT TRANSFER. Vol.5, Princeton Series on High Speed Aerodynamics and Jet Propulsion. Princeton University press, 1959.
14. Sigalla, A. "Experiments with Pitot Tubes for Skin Friction Measurements." British ..Iron and Steel Research Association Report P/2/58, List 92, 1958.
15. Klebanoff, P.S. "Characteristics of Turbulence in a Boundary Layer with Zero Pressure Gradient." NACA Report 1247, 1955.
16. Rubesin, M. W., Maydew, R. C., and Varga, S. A. "An Analytical and Experimental Investigation of Skin Friction of the Turbulent Boundary Layer on a Flat Plate at Supersonic Speeds." NACA TN 2305, February, 1951.
17. Duncan, W. J., Thom, A. S.,Young, A. D., MECHANICS OF FLUIDS, American Elsevier Publishing Co. New York, 1970.
18. Rumsey, C, L., Biedron, R. T. and Thomas, J. L., “CFL3D: Its History and Some Recent Applications”, NASA TM-112861, 1997
19. Rivers, M. B. and Wahls, R. A., “Turbulence Model Comparisons for a High-Speed Aircraft”, NASA CDTP-1012, November 1997, NASA/TP-1999-209540, Dec. 1, 199, LaRC
20. Bardina, J. E., Huang, P. G. and Coakley, T. J., “Turbulence Modeling Validation, Testing, and Development”, NASA TM-110446, April 1977
21. Baldwin, B. and Lomax, H., “Thin-Layer Approximation and Algebraic Model for Separated Turbulent Flows”, AIAA-78-257, January 1978
22. Degani, D., Schiff, L. B.and Levy, Y., “Physical Considerations Governing Computation of Turbulent Flows”, AIAA-90-0096, January 1990
23. Spalart, P. R. and Allmaras, S. R., “A One-Equation Turbulence Model for Aerodynamic Flows”, AIAA-92-0439, January 1992
24. Menter, F. R., “Assessment of Two-Equation Turbulence Models for Transonic Flows”, AIAA 94-2343, June 1994
25. Menter, F. R., “Two-Equation Eddy-Viscosity Turbulence Models for Engineering Applications:, AIAA Journal, vol. 32, no. 8, August 1994, pp. 357-372
26. Chan, W. M. and Buning, P. G., “Users Manual for FOMOCO Utilities – Force and Moment Computational Tools for Overset Grids”, NASA TM=110408, 1996
27. Ashkenas, H., and Riddell, F. R. "Investigation of the Turbulent Boundary Layer on a Yawed Flat Plate." NACA TN 3383, 1955.
28. Klebanoff, P.S., and Diehl, Z. E. "Some Features of Artificially Thickened Fully Developed Boundary Layers with Zero Pressure Gradient." NACA Report 1110, 1952.

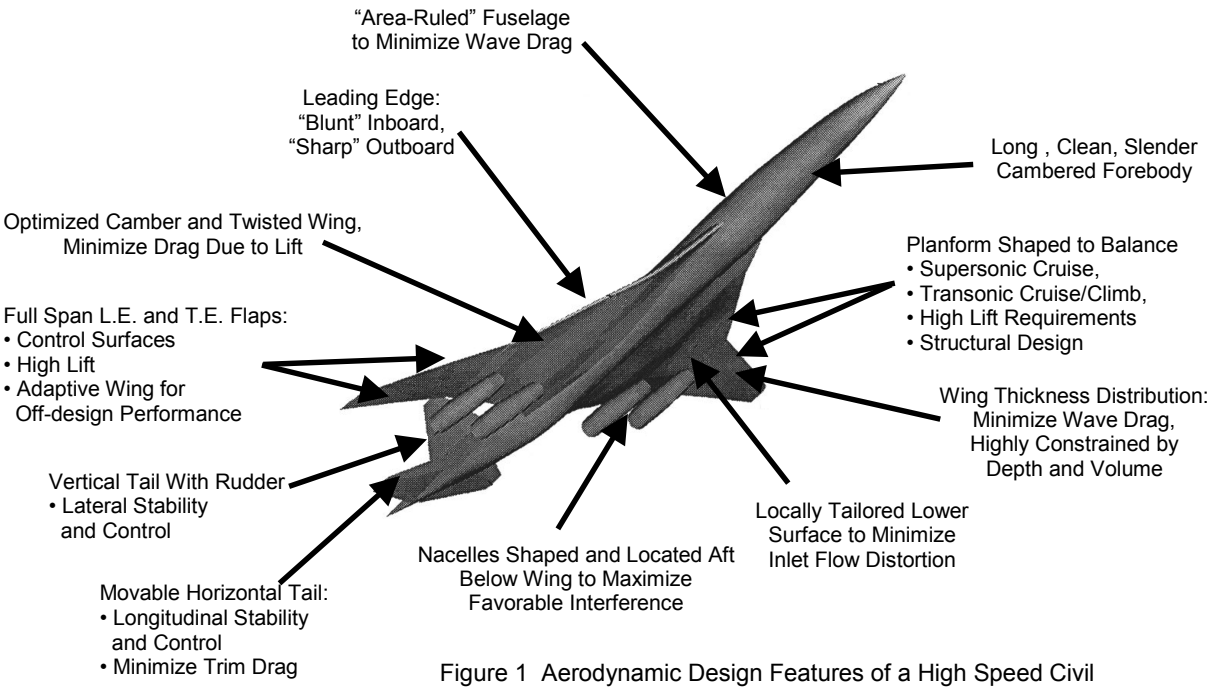

Figure 1 Aerodynamic Design Features of a High Speed Civil

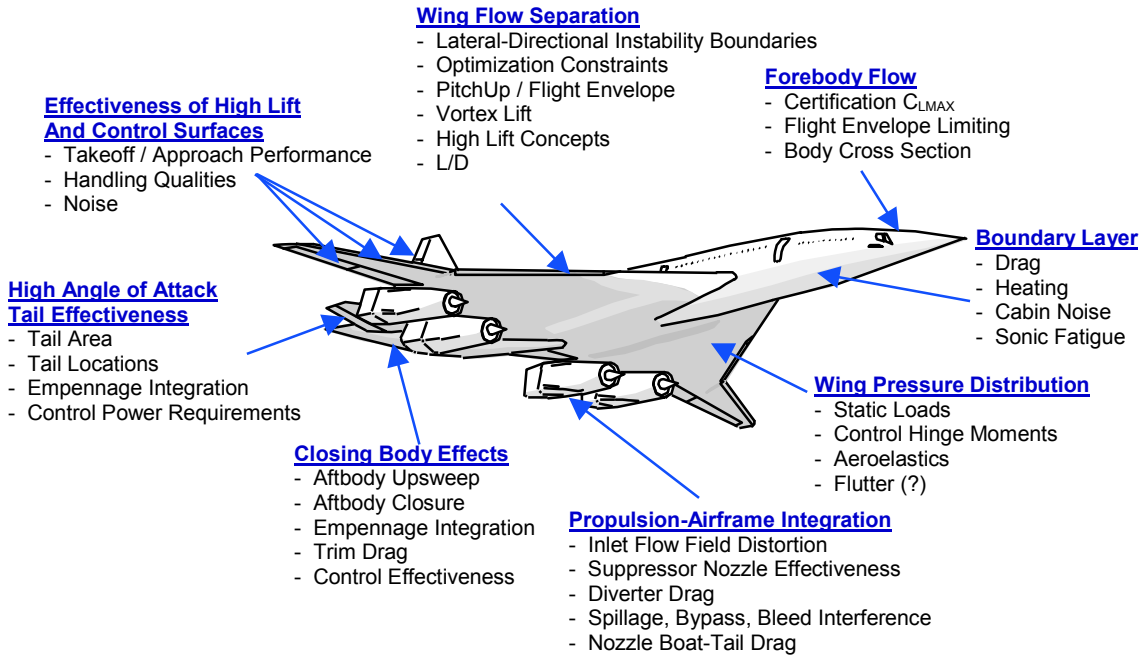

Figure 2 Aerodynamic Design Features Affected by Reynolds

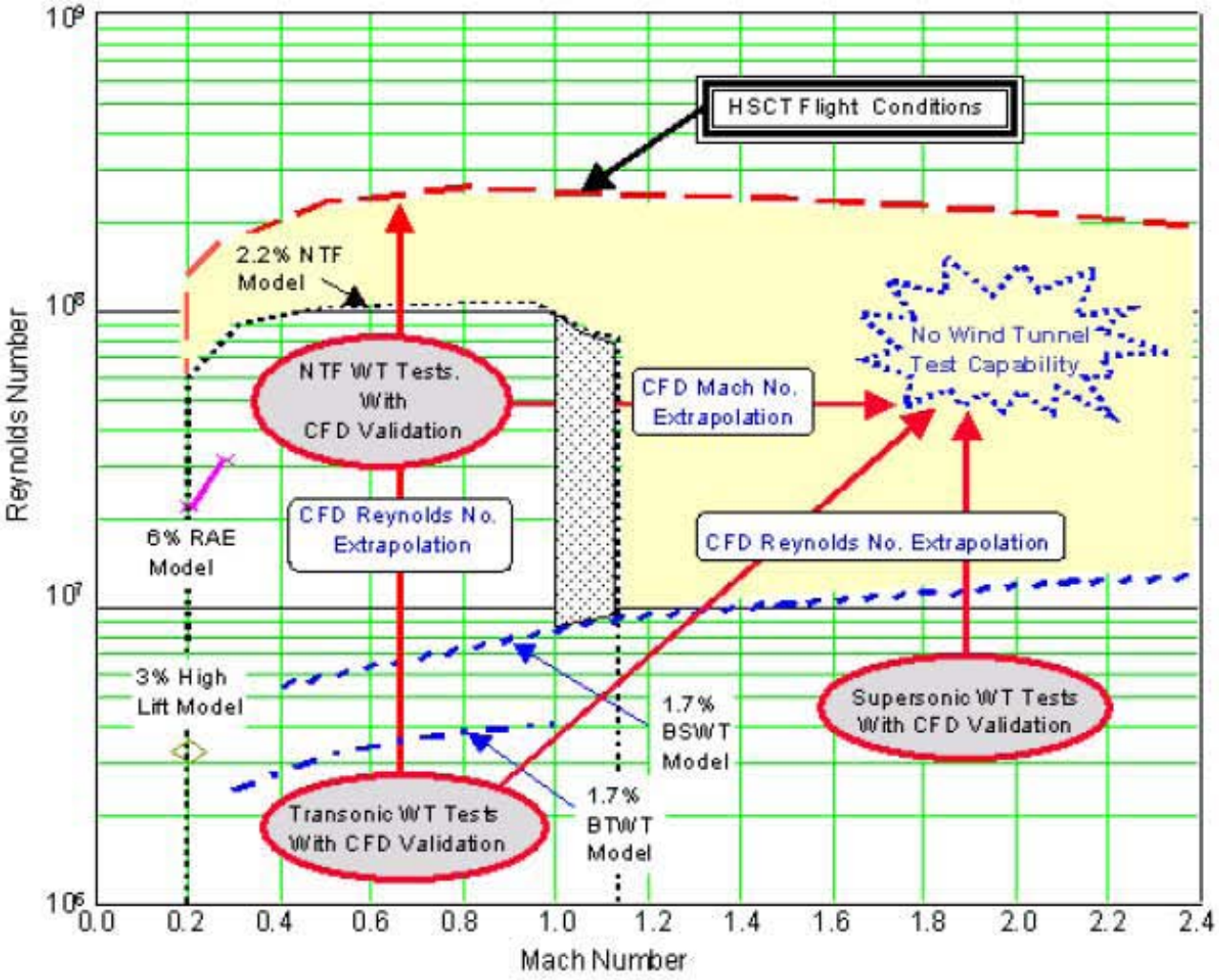

Figure 3 Testing Capability and Full Scale Prediction Strategy

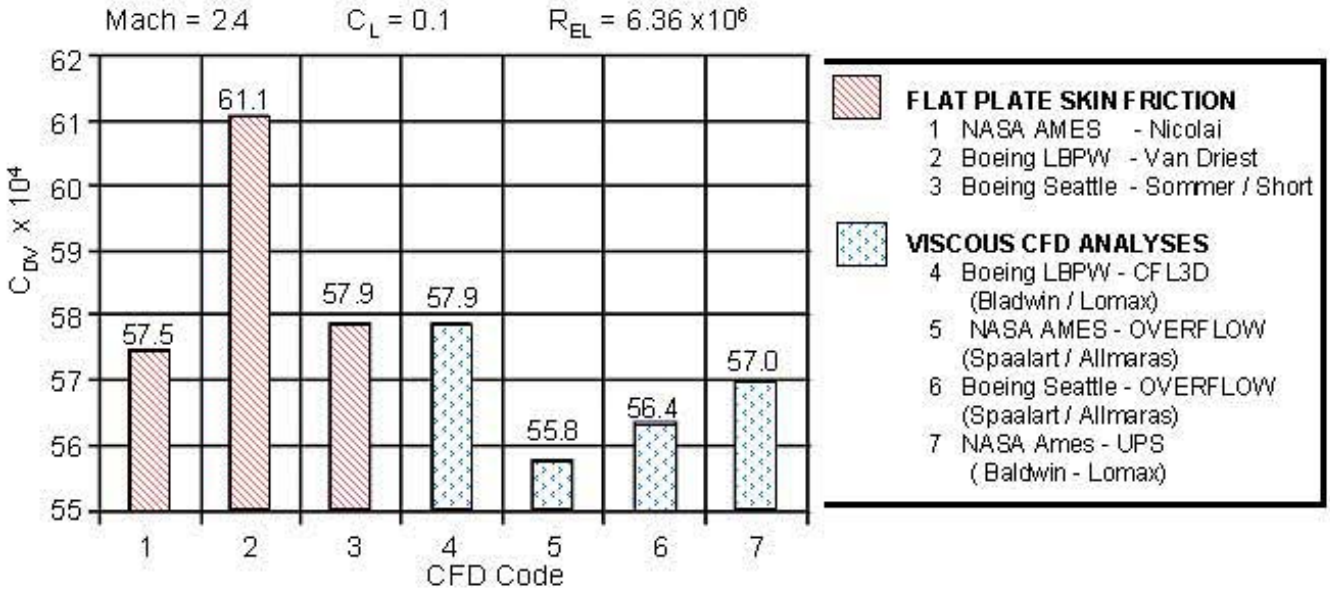

Figure 4 Comparisons of Fully Turbulent Flow Viscous Drag Predictions - Typical HSCT Wing / Body

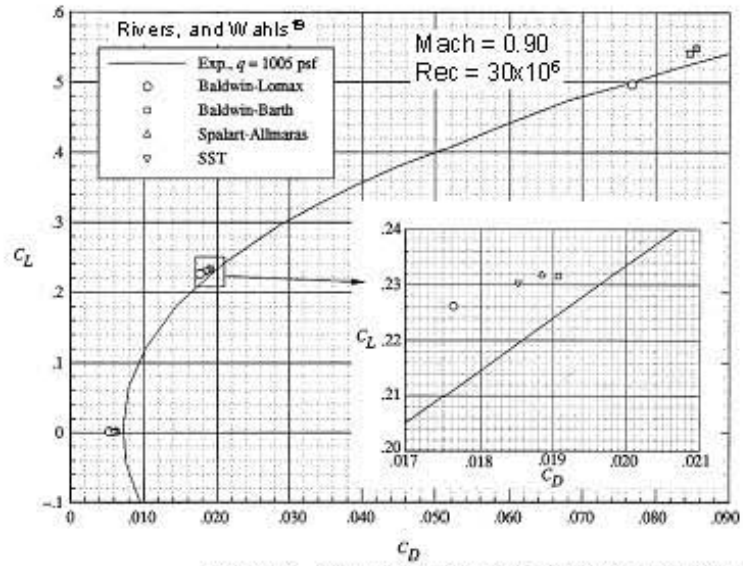

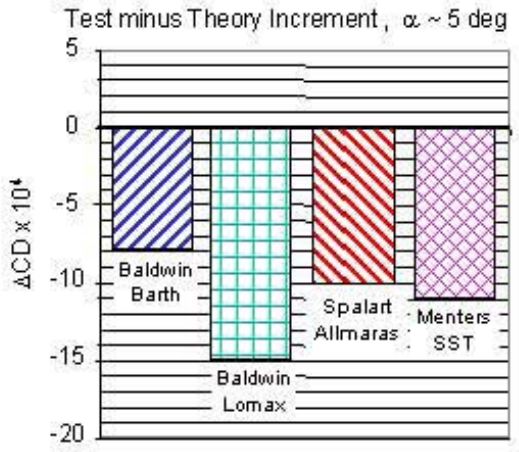

Figure 5, Drag Prediction With CFD Viscous Drag

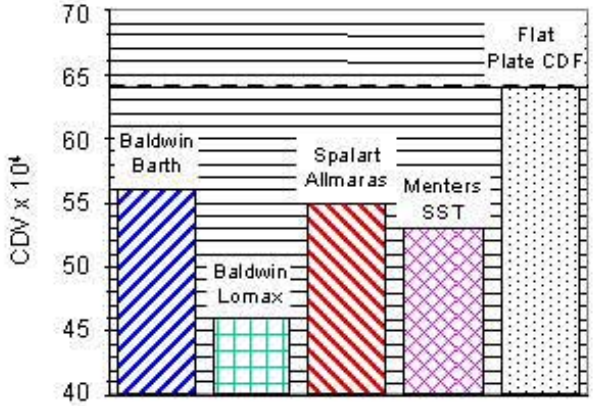

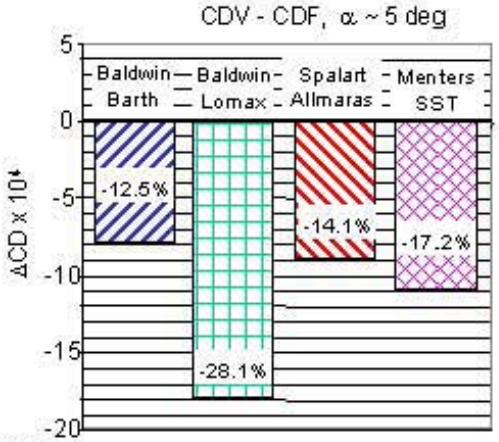

Figure 6, Viscous Drag Predictions

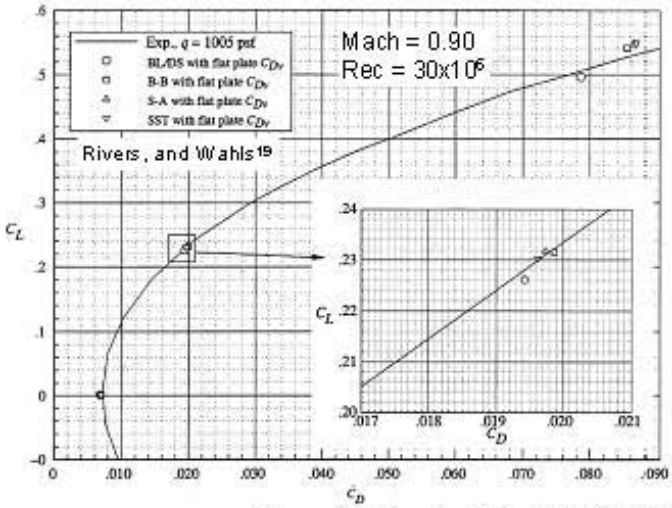

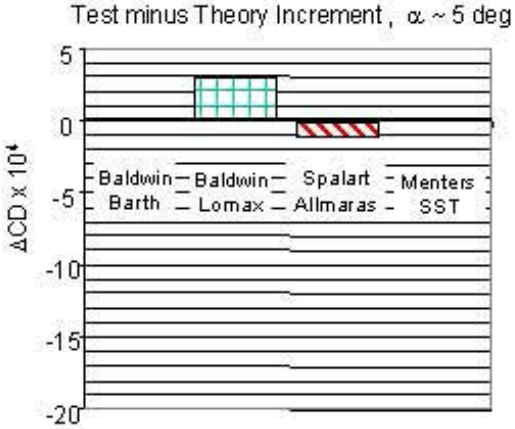

Figure 7, Drag Prediction With Flat Plate Skin Friction Viscous Drag

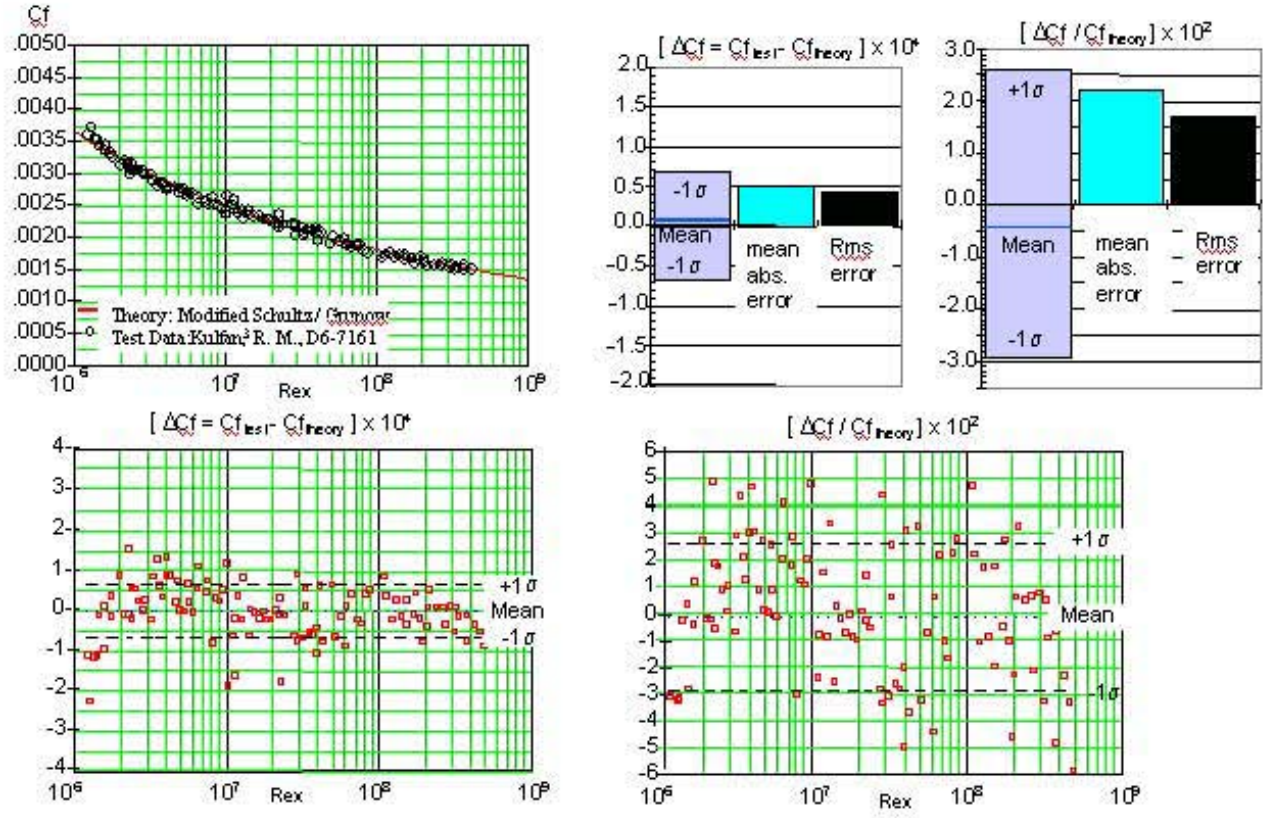

Figure 8 Incompressible Local Skin Friction Data

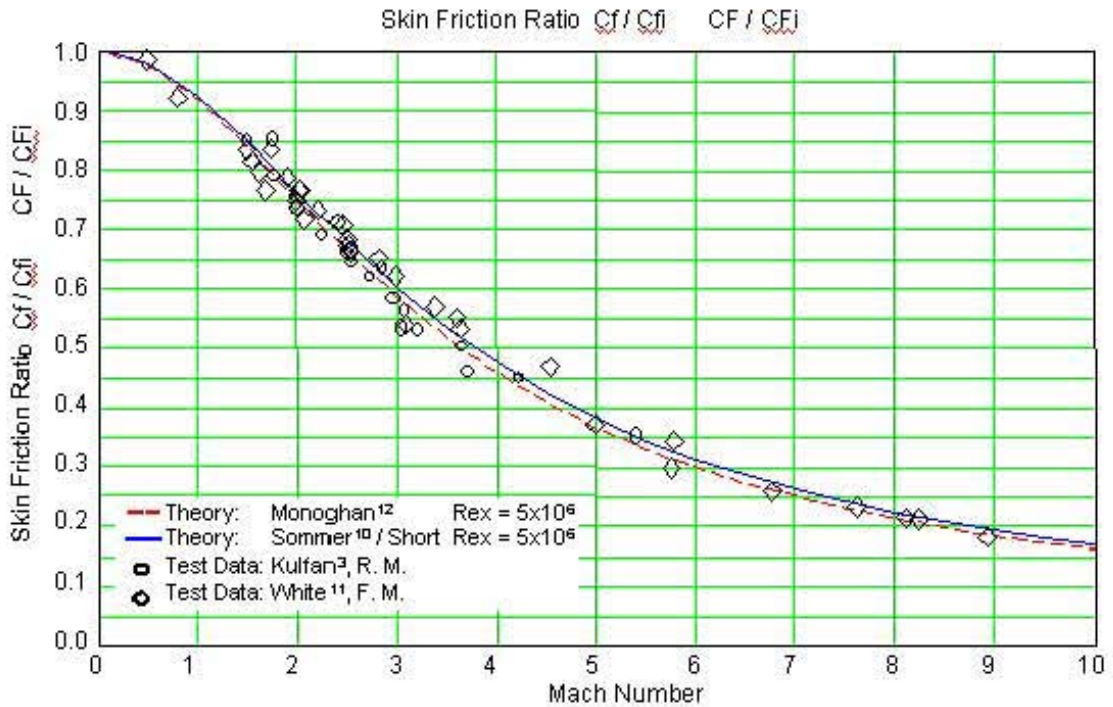

Figure 9 Comparison of Compressibility Effects Predictions

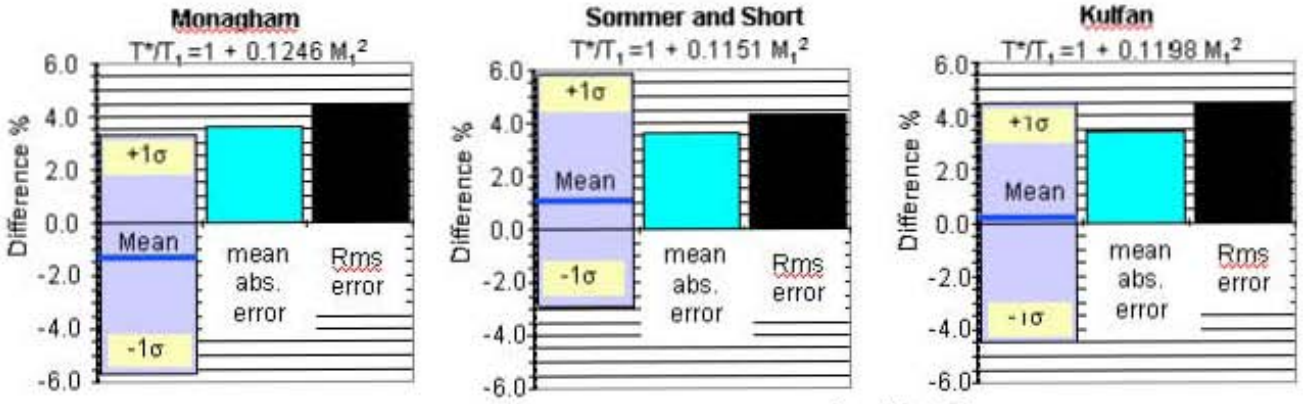

Figure 10 Percent Variation Between test and Prediction $\left[\frac{\Delta Cf/Cfi}{Cf/Cfi}\right]*10^2$

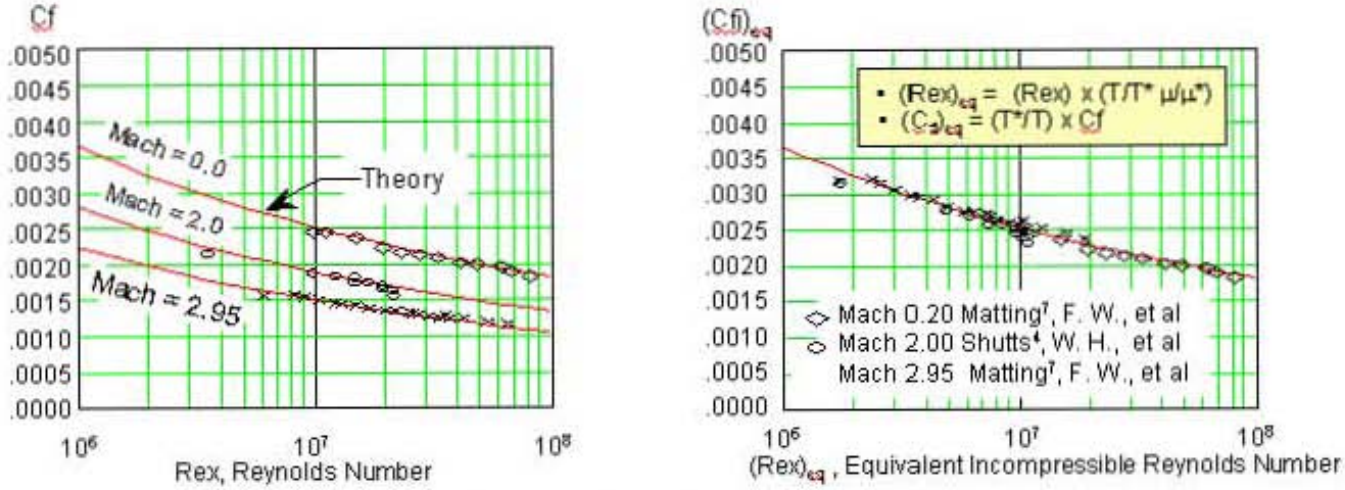

Figure 11 Conversion of Cf Data To Equivalent Incompressible Data

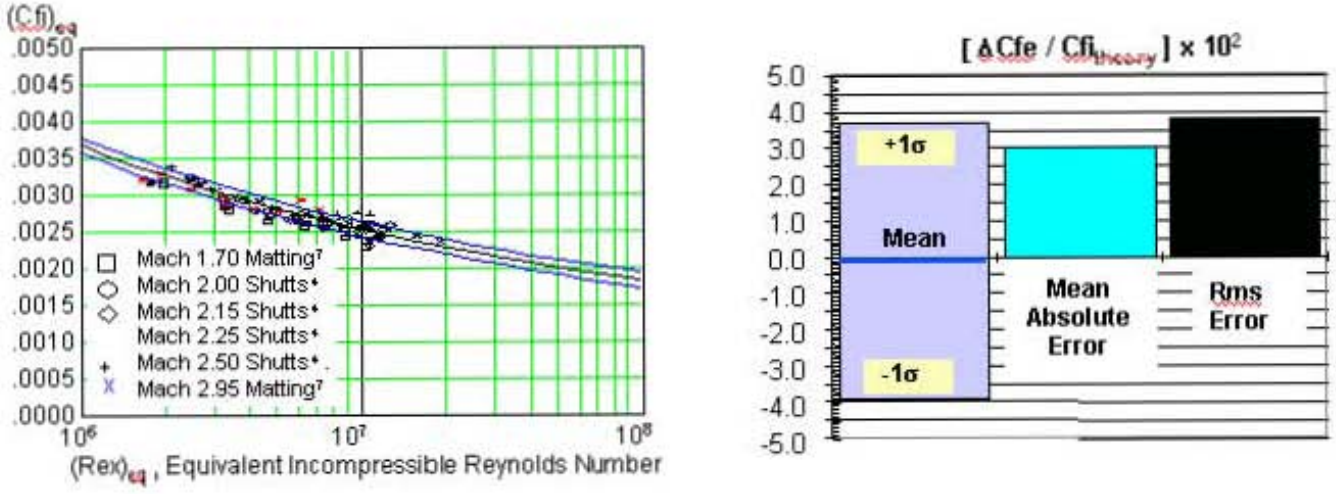

Figure 12 Conversion of Supersonic Cf Data To Equivalent Incompressible Data

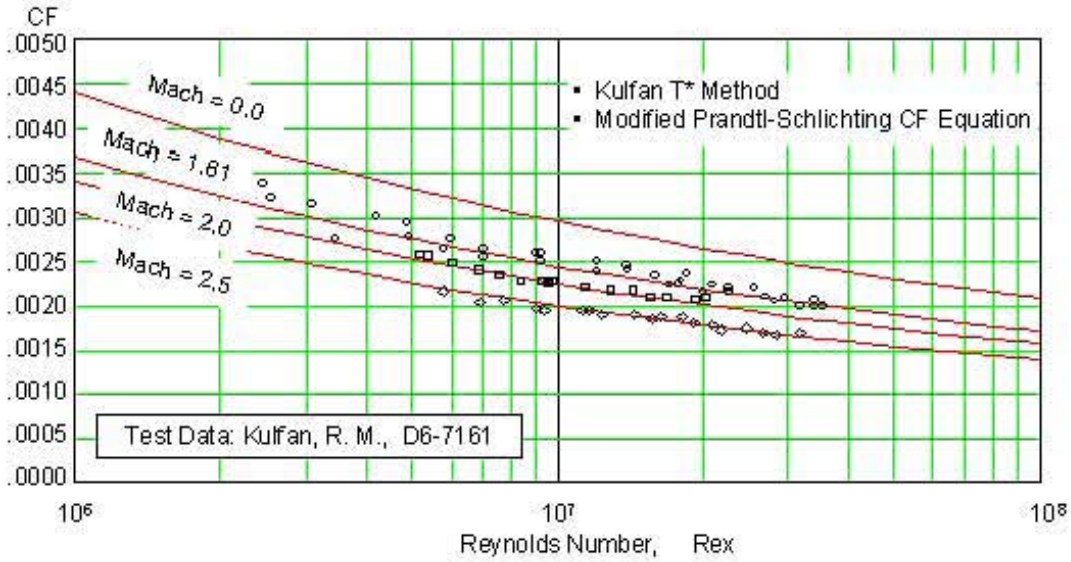

Figure 13 Average Skin Friction Coefficient: Test vs Theory

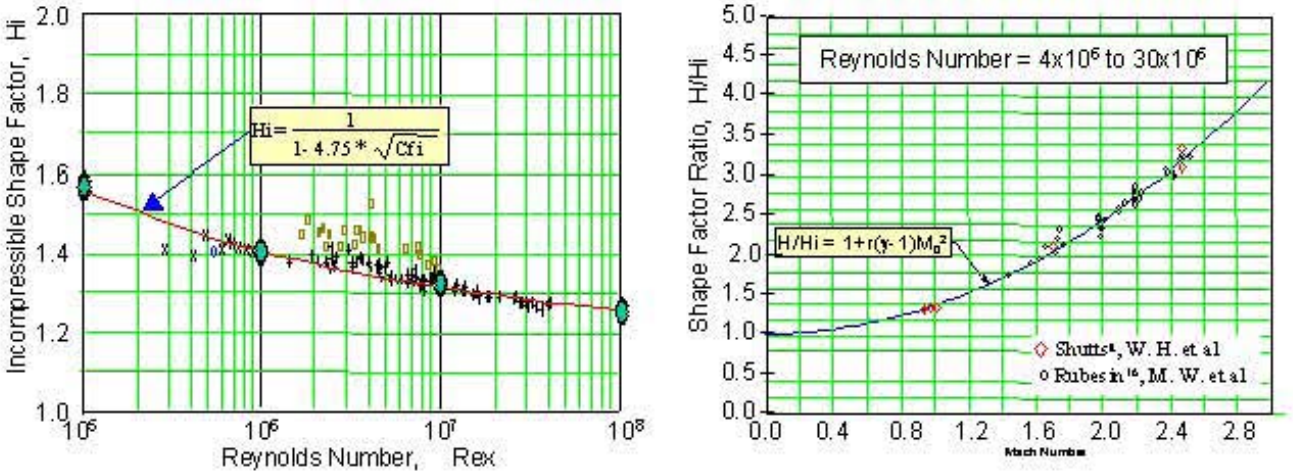

Figure 14 Flat Plate Turbulent Flow Shape Factor

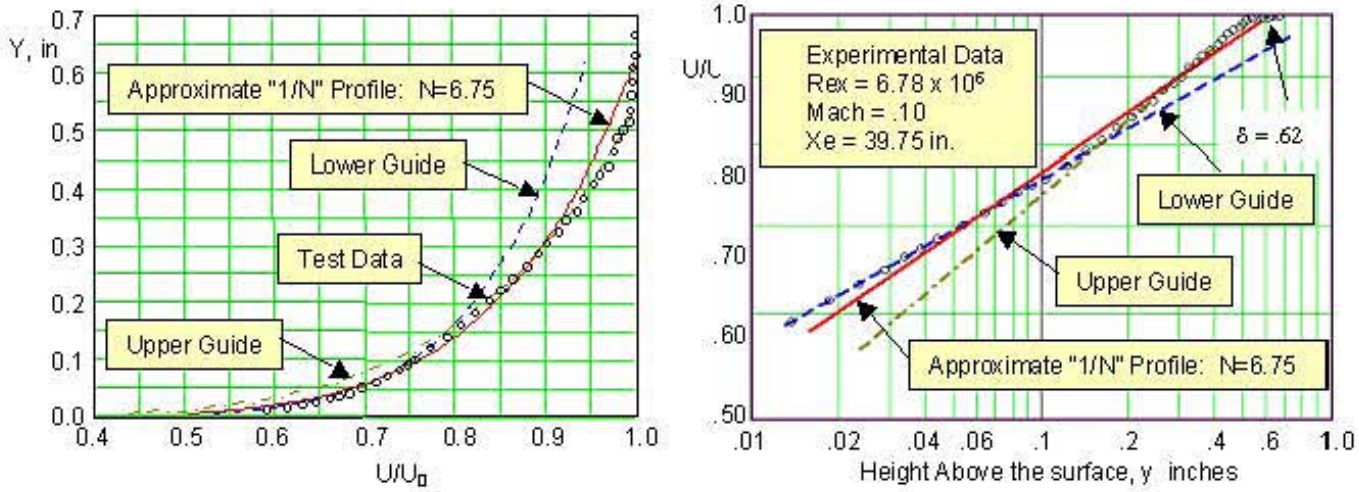

Figure 15 Typical Flat Plate Turbulent Flow Velocity Profile Data

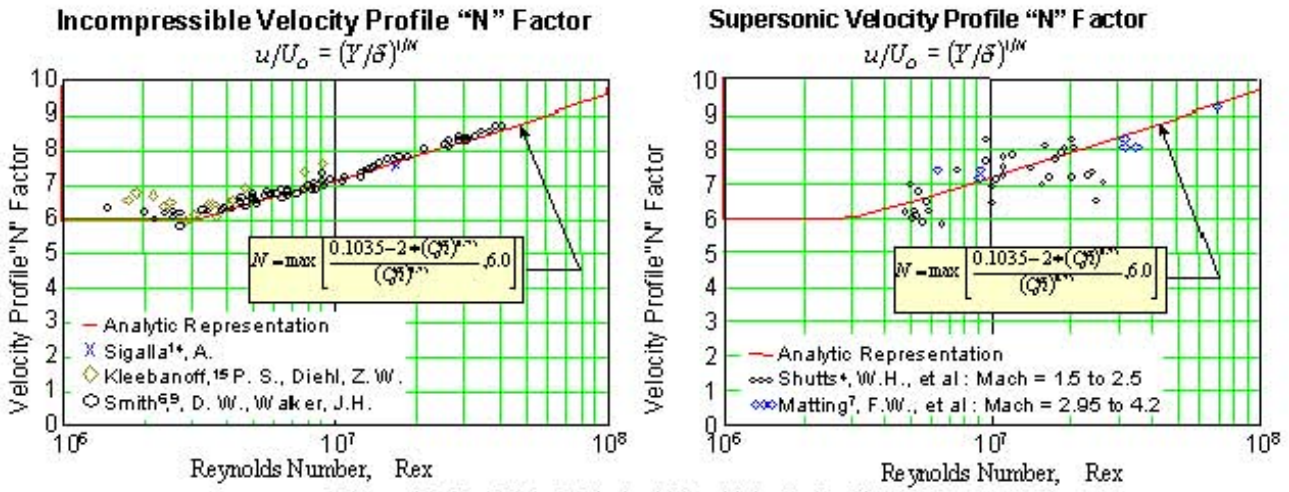

Figure 16 Flat Plate Turbulent Flow Velocity Profile Factor

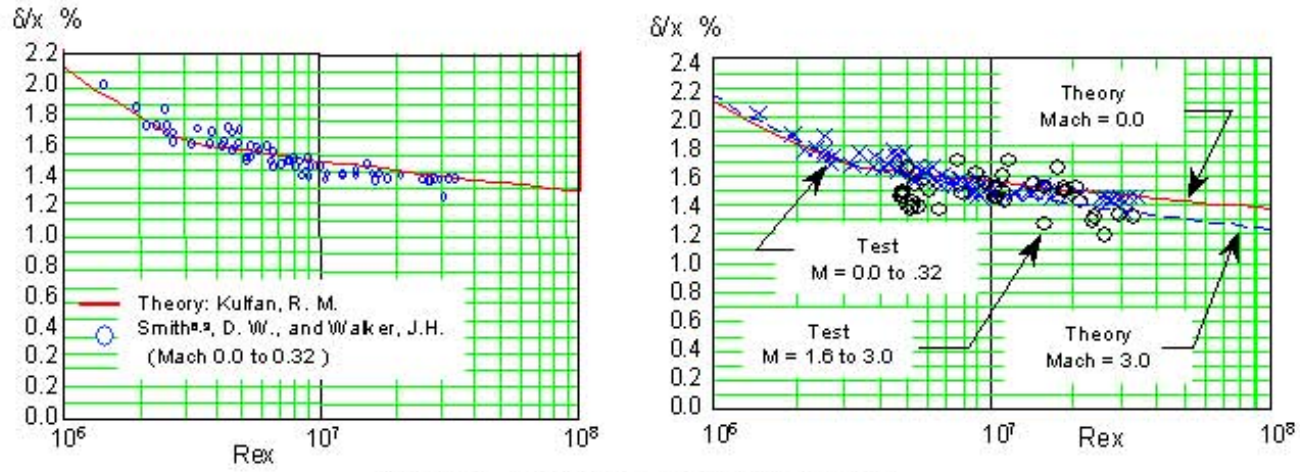

Figure 17 Boundary Layer Thickness, δ/x (%)

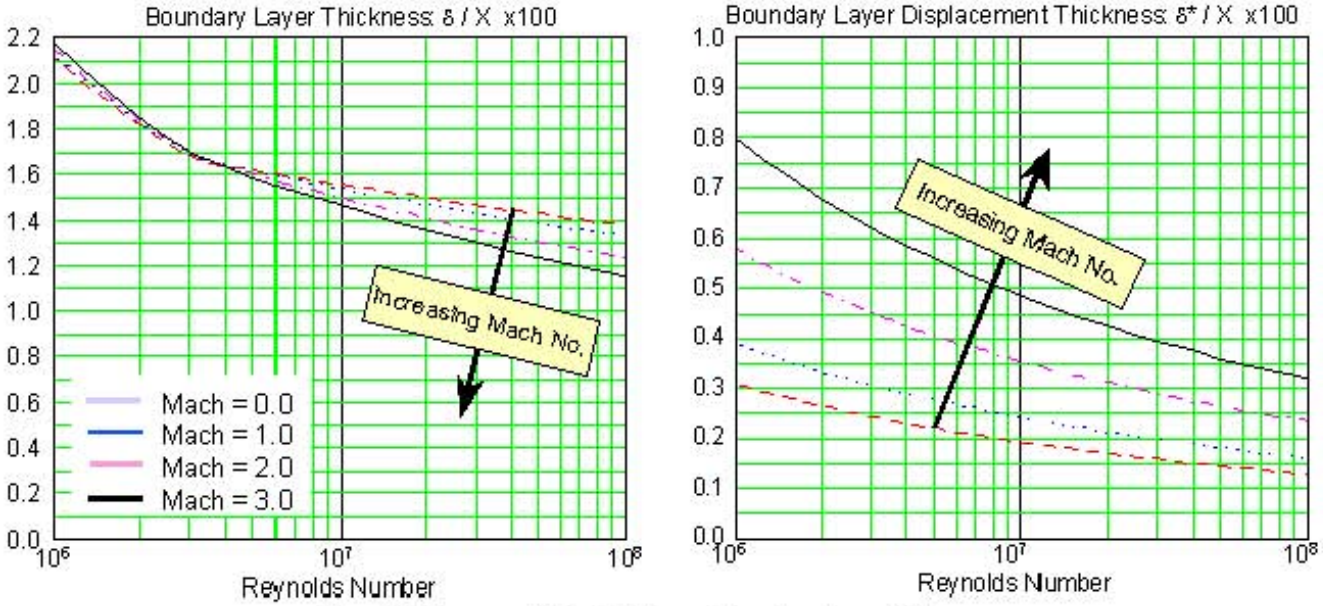

Figure 18 Compressibility Effects on Boundary Layer Thickness

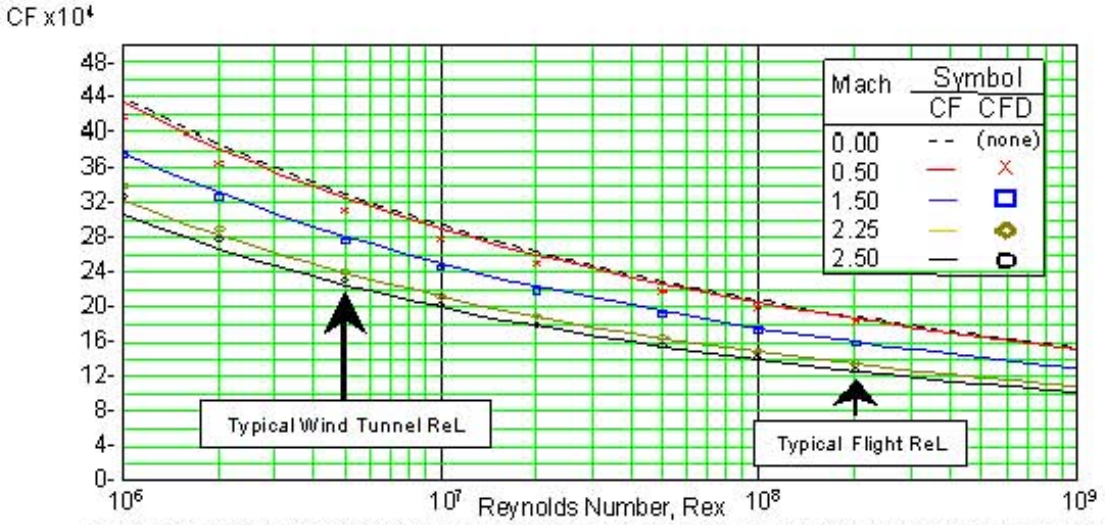

Figure 19 BPW-LB CFL3D: Average Skin friction Calculations; Baldwin-Lomax Turbulence Model

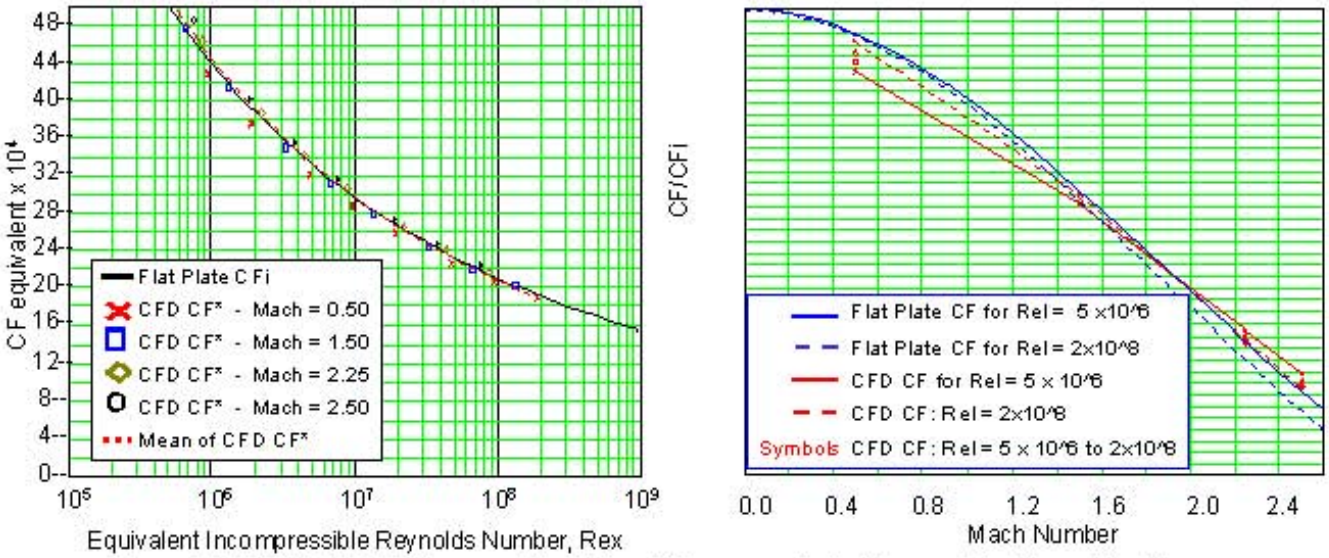

Figure 20 BPW-LB CFL3D: Average Skin friction Differences; Baldwin-Lomax Turbulence Model

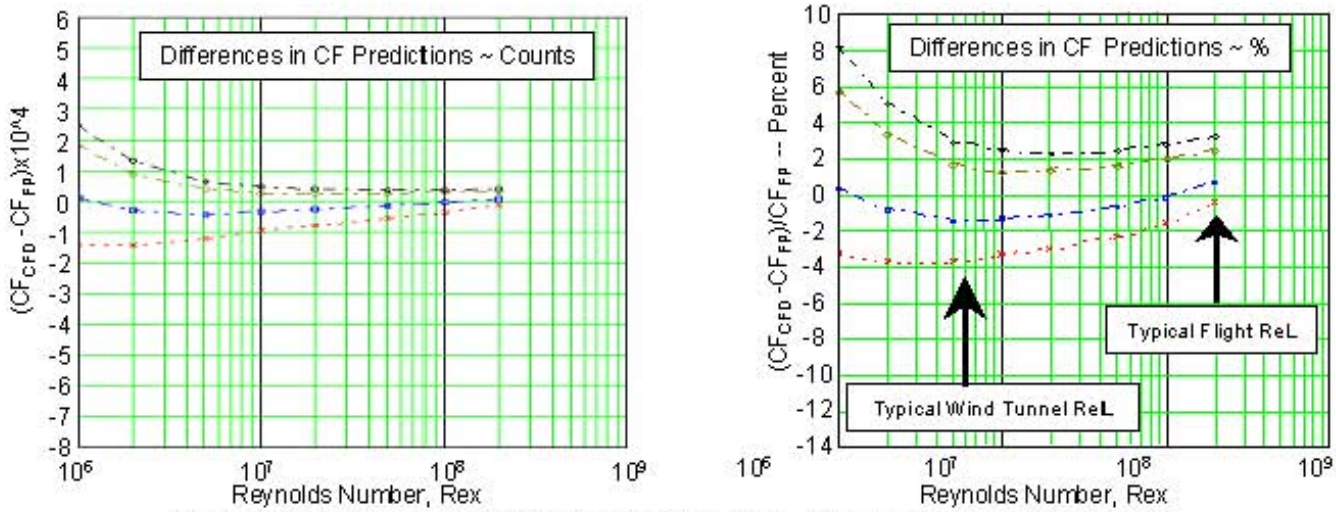

Figure 21 BPW-LB CFL3D: Average Skin friction Trends; Baldwin-Lomax Turbulence Model

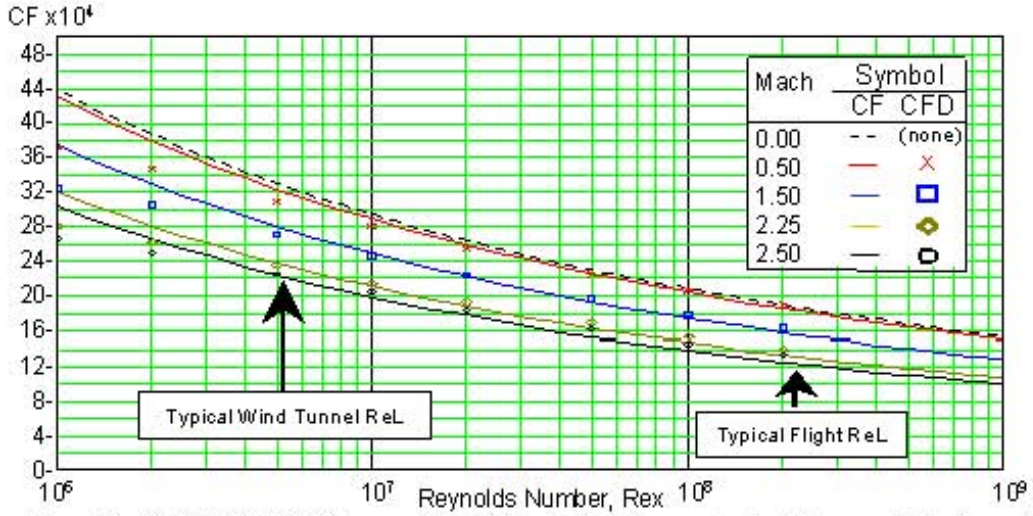

Figure 22 BPW-LB CFL3D: Average Skin friction Calculations; Spalart-Allmaras Turbulence Model

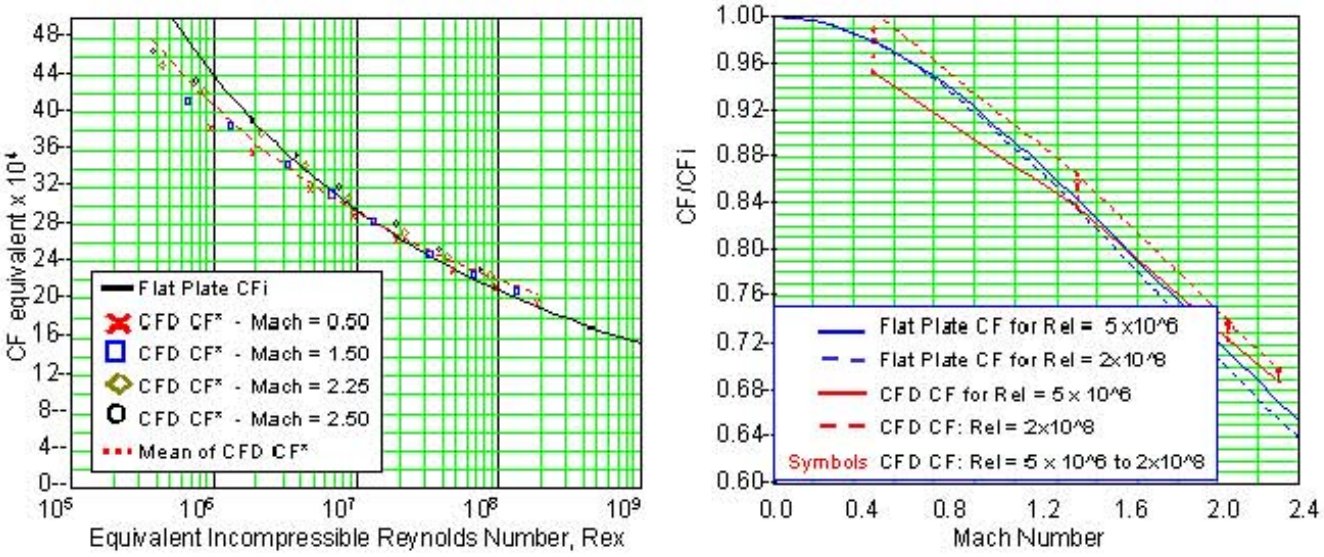

Figure 23 BPW-LB CFL3D: Average Skin friction Trends; Spalart-Allmaras Turbulence Model

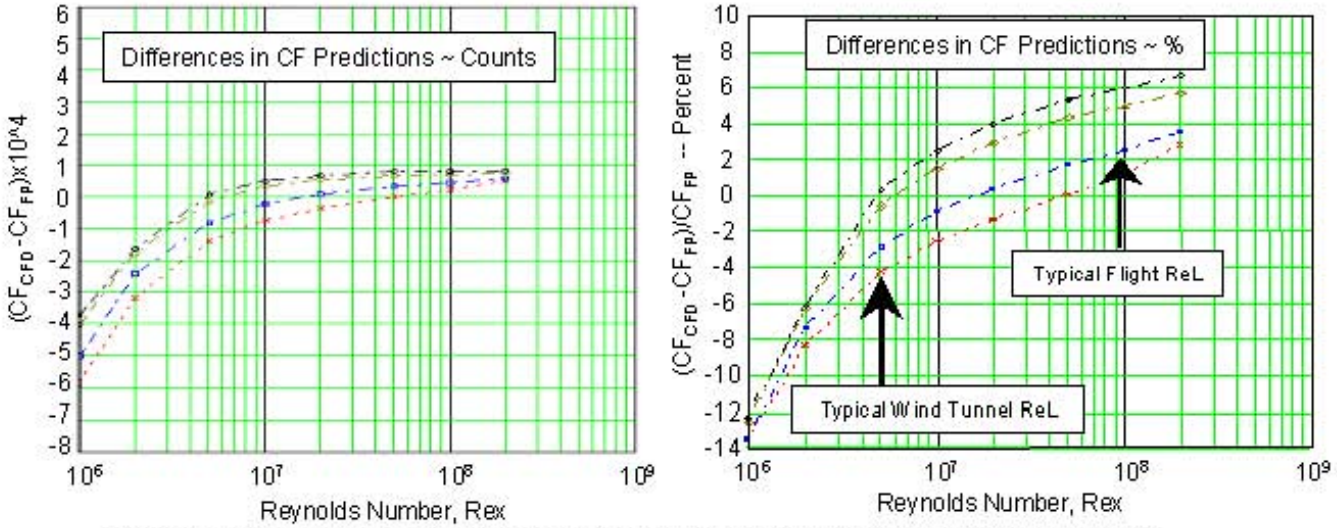

Figure 24 BPW-LB CFL3D: Average Skin friction Differences; Spalart-Allmaras Turbulence Model

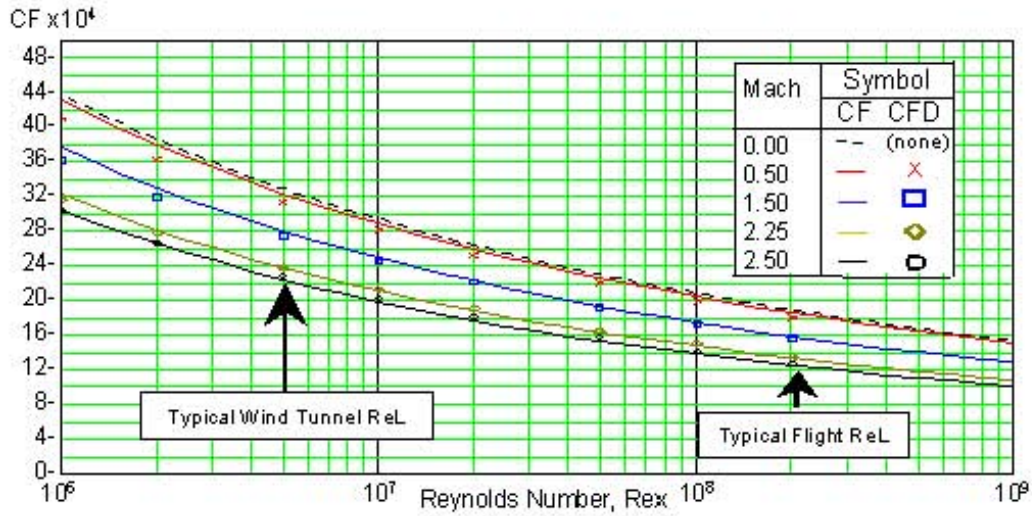

Figure 25 BPW-LB CFL3D: Average Skin friction Calculations; Menter's SST Turbulence Model

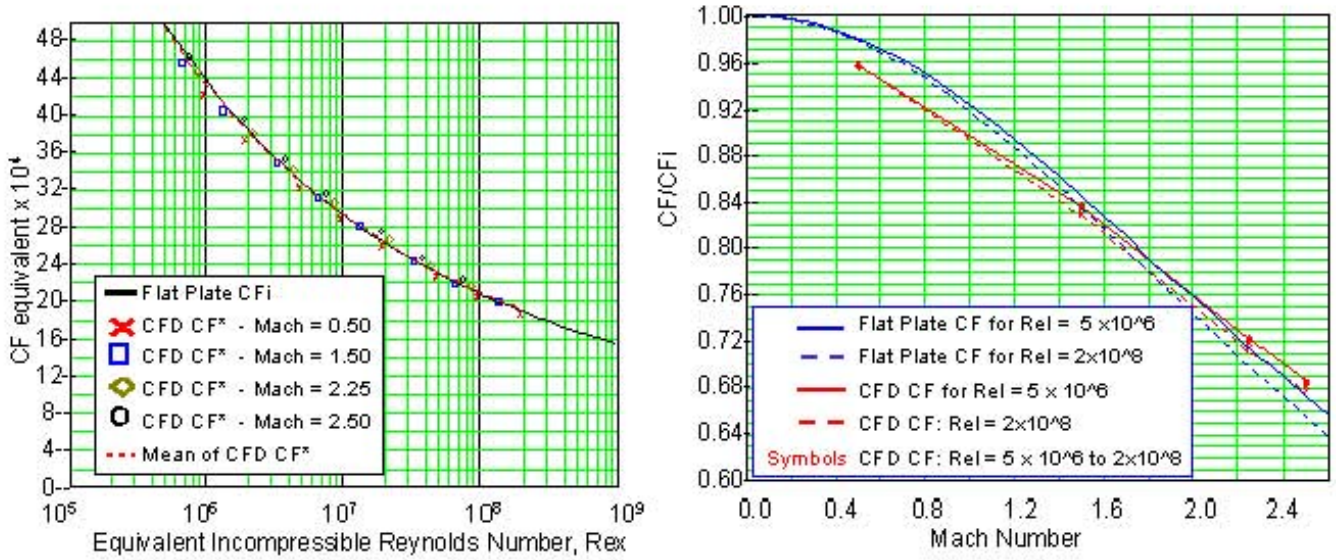

Figure 26 BPW-LB CFL3D: Average Skin friction Trends; Menter's SST Turbulence Model

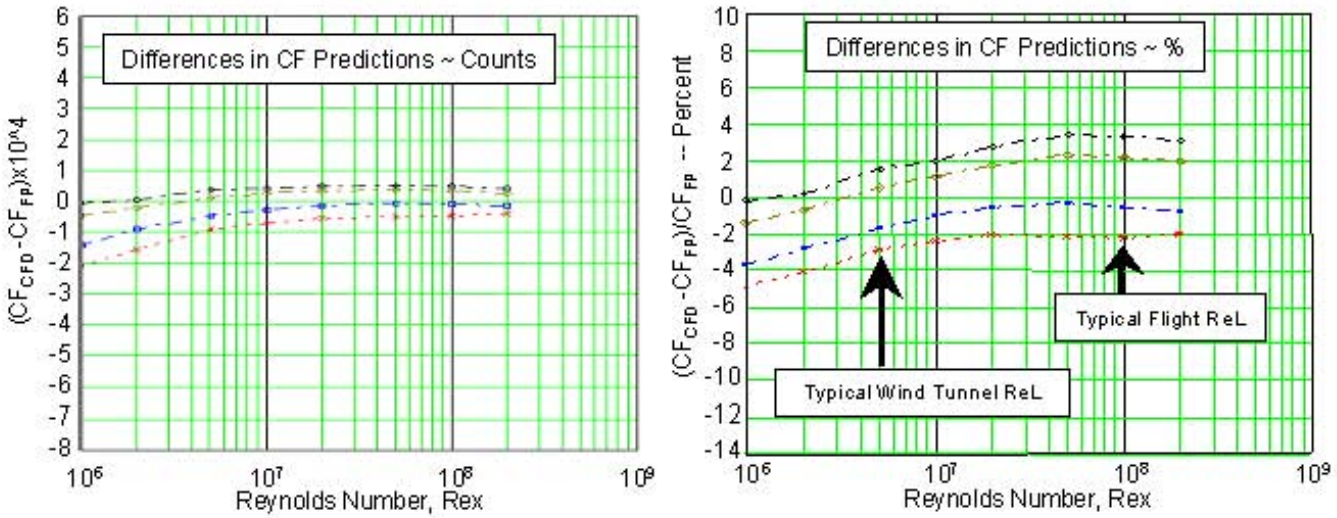

Figure 27 BPW-LB CFL3D: Average Skin friction Differences; Menter's SST Turbulence Model

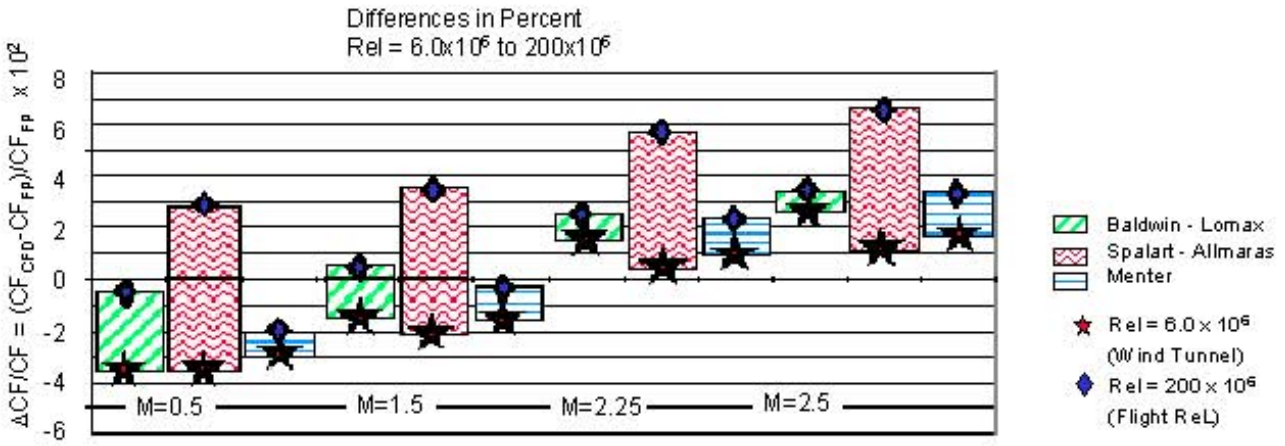

Figure 28 Summary of BPW-LB Viscous Drag Predictions Compared with Flat Plate Data

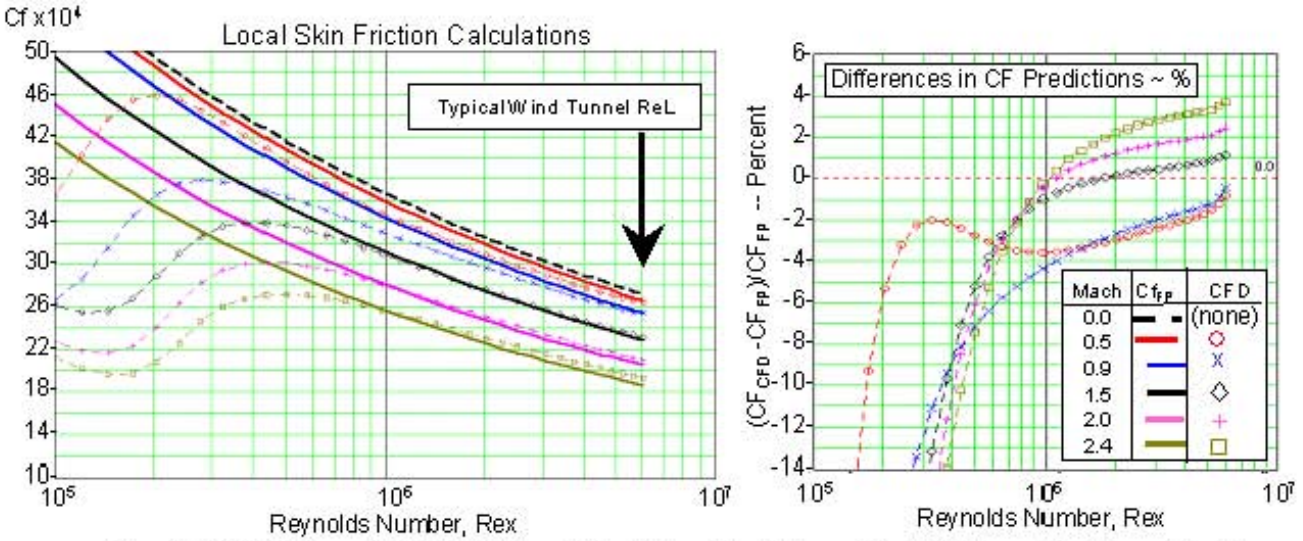

Figure 29 NASA Ames OVERFLOW: Local Skin friction Calculations; Spalart-Allmaras Turbulence Model

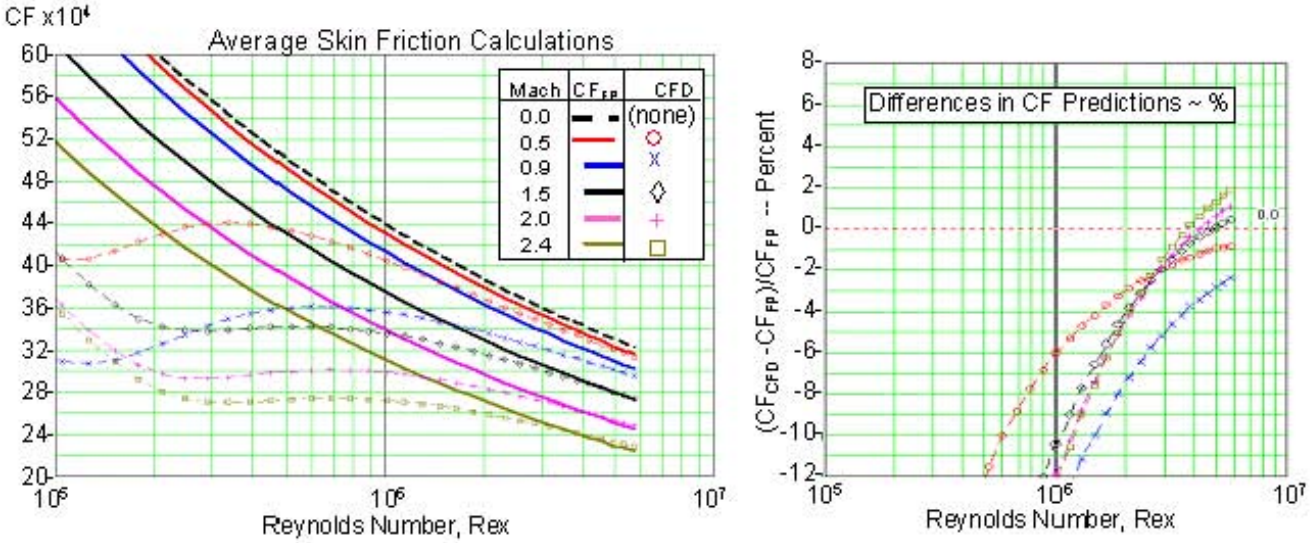

Figure 30 NASA Ames OVERFLOW: Average Skin friction Calculations; Spalart-Allmaras Turbulence Model

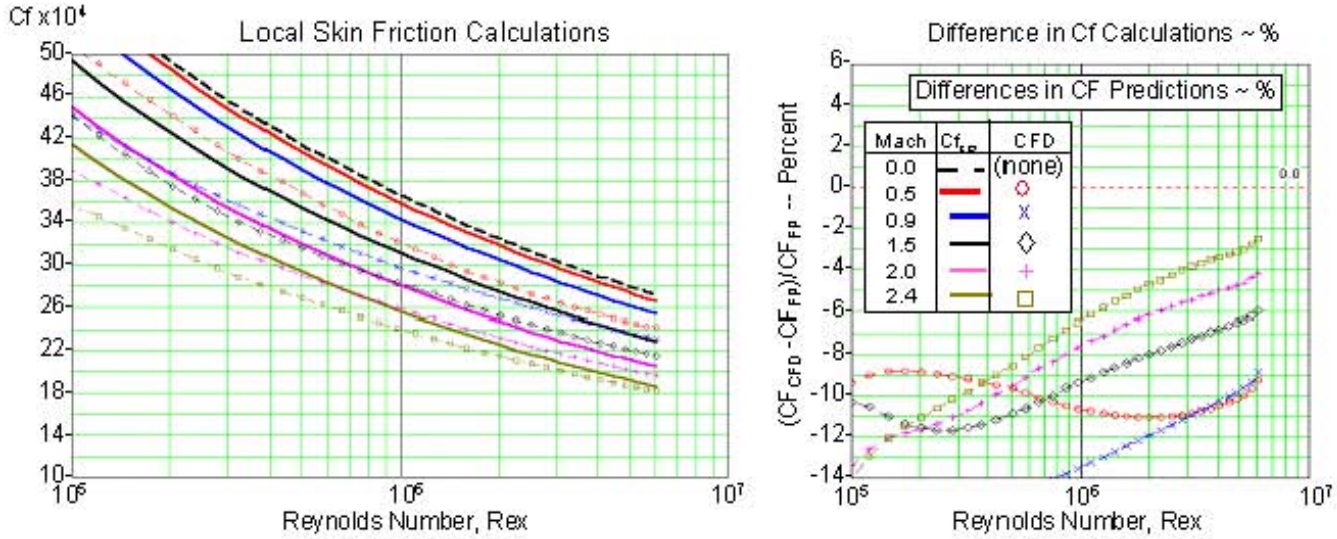

Figure 31 NASA Ames OVERFLOW: Local Skin friction Calculations; Menters Turbulence Model

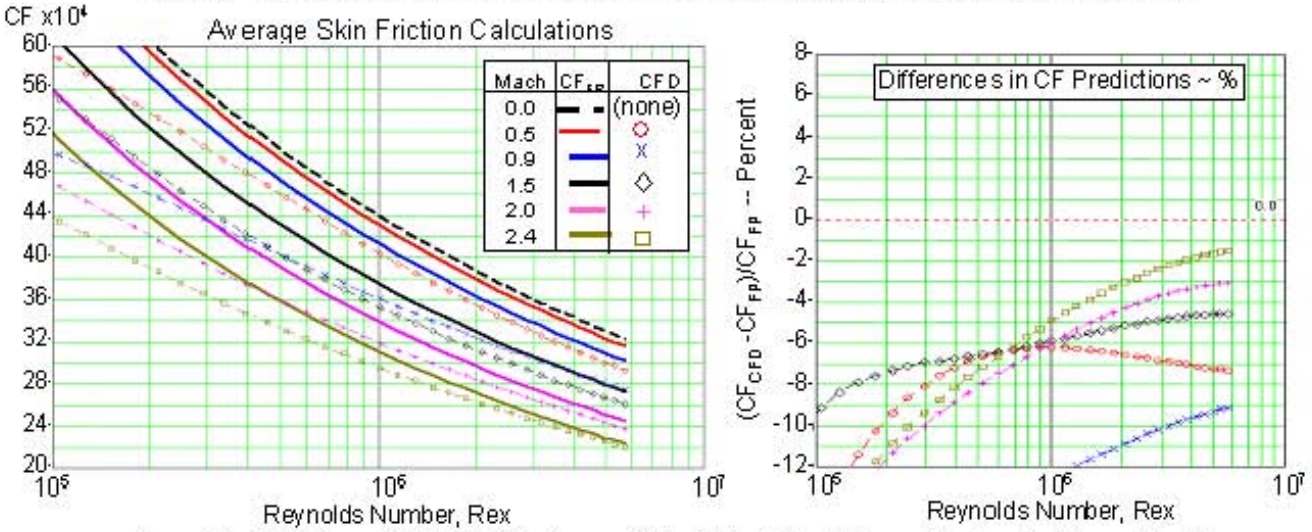

Figure 32 NASA Ames OVERFLOW: Average Skin friction Calculations; Menters Turbulence Model

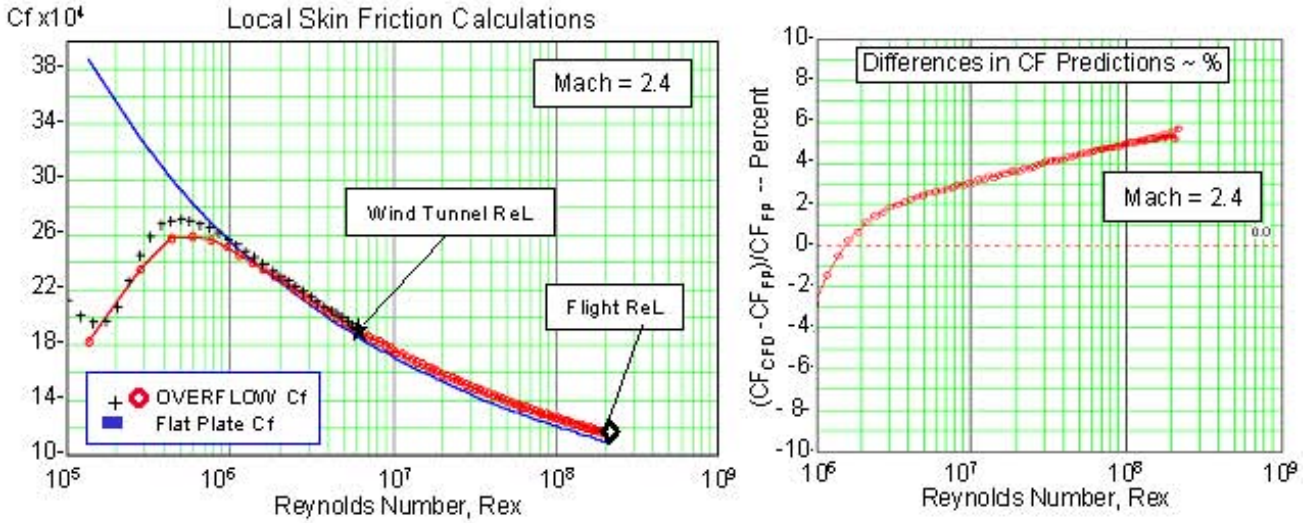

Figure 33 NASA Ames OVERFLOW: Local Skin friction Calculations; Spalart - Allmaras Turbulence Model

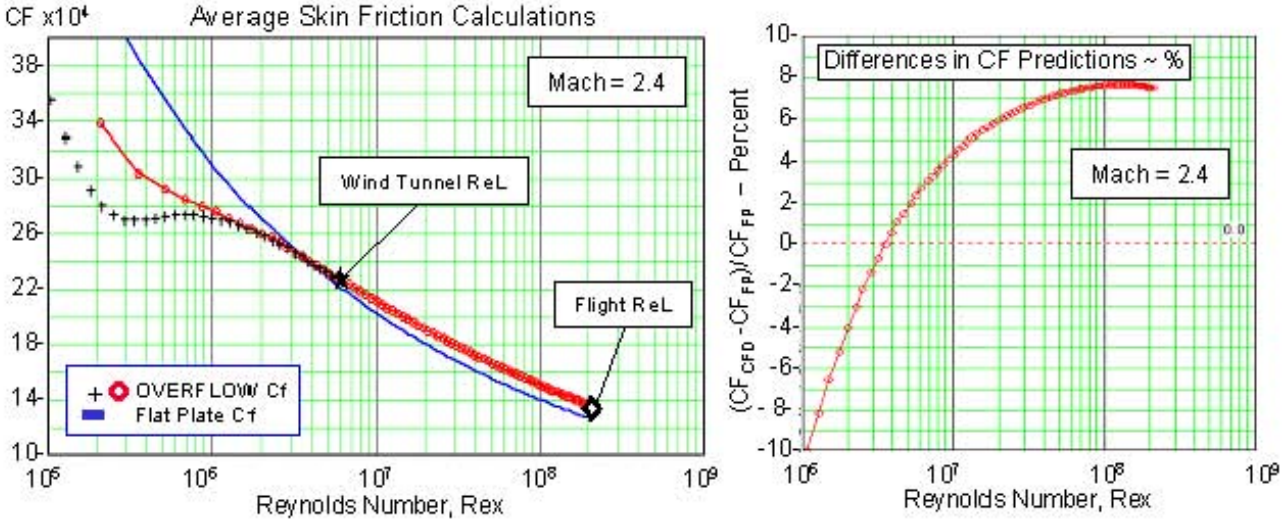

Figure 34 NASA Ames OVERFLOW:Average Skin friction Calculations; Spalart - Allmaras Turbulence Model

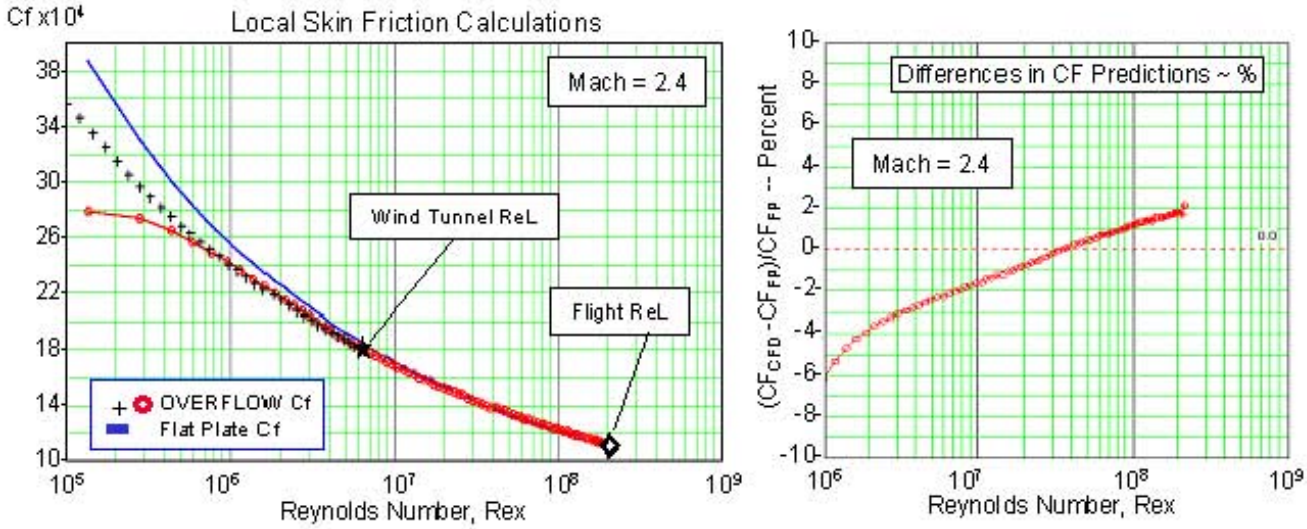

Figure 35 NASA Ames OVERFLOW: Local Skin friction Calculations; Menter's SST Turbulence Model

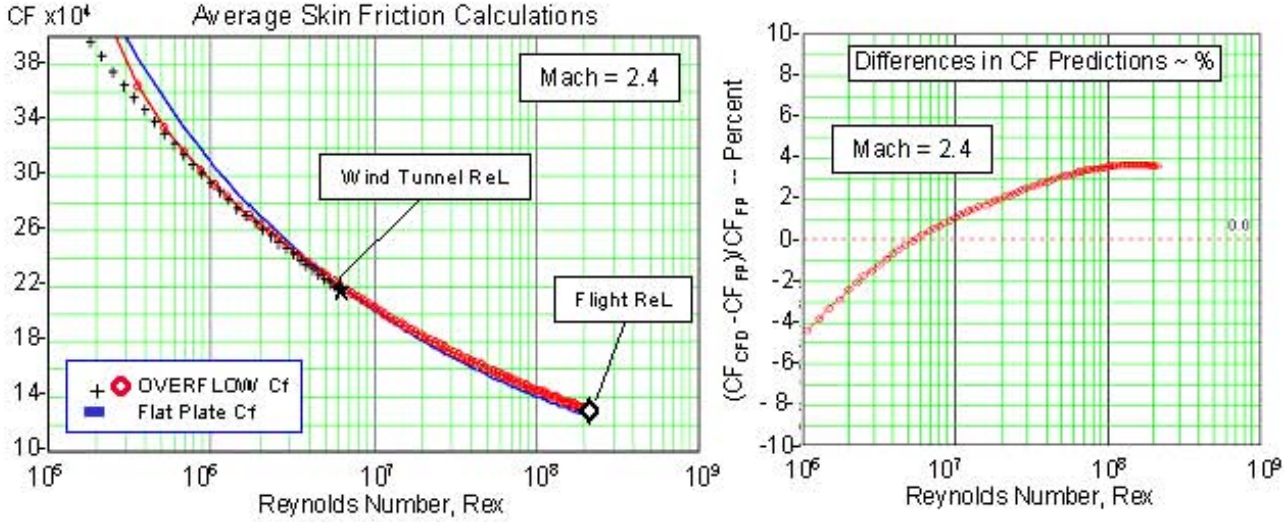

Figure 36 NASA Ames OVERFLOW:Average Skin friction Calculations; Menter's SST Turbulence Model

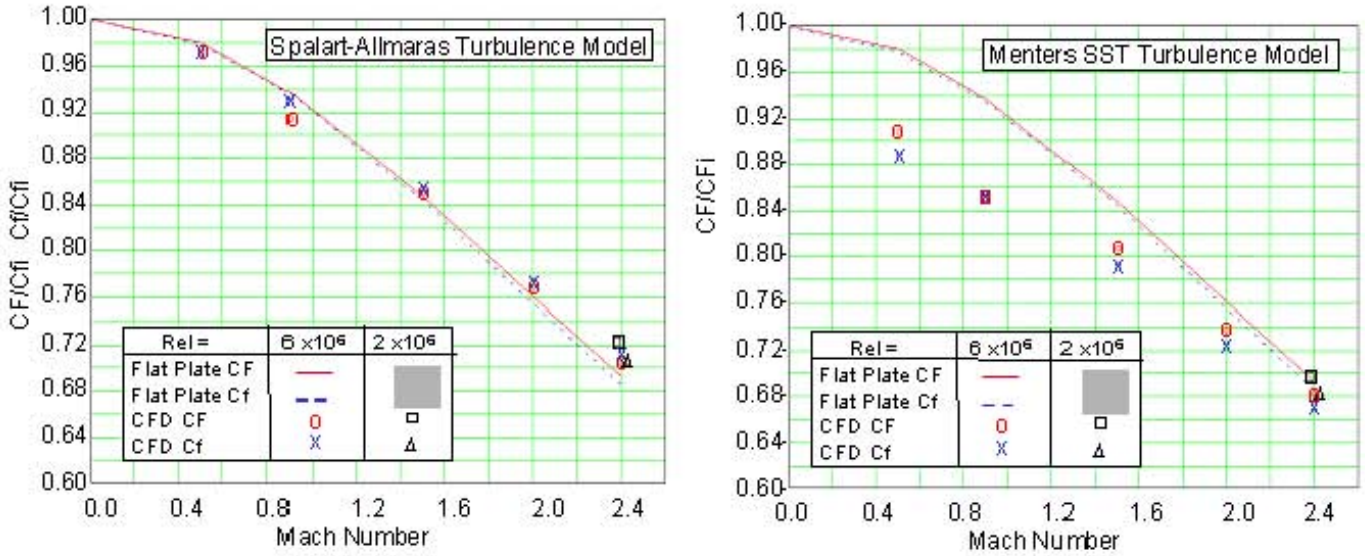

Figure 37 NASA Ames OVERFLOW: Local and Average Skin friction Variation with Mach number

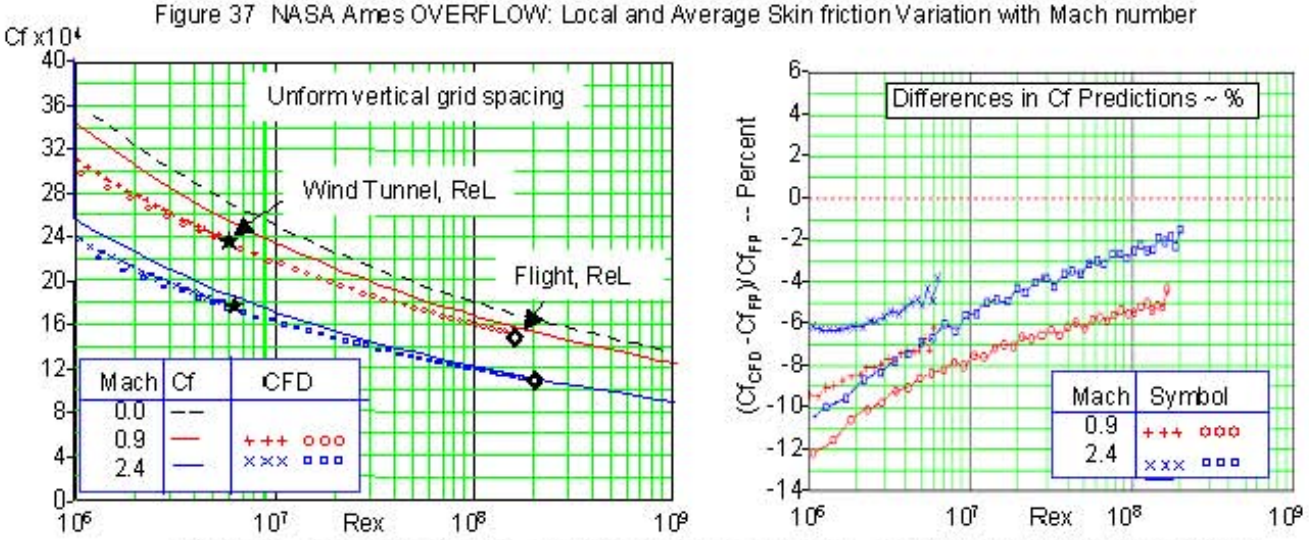

Figure 38 BCAG OVERFLOW Local Skin friction Calculations; Baldwin - Lomax Turbulence Model

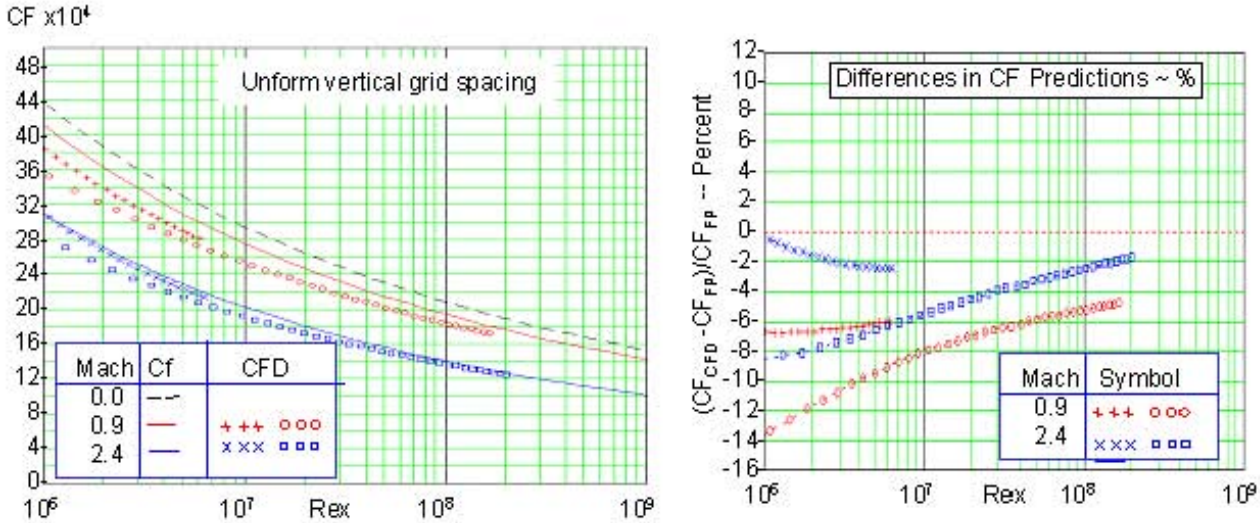

Figure 39 BCAG OVERFLOW: Average Skin friction Calculations; Baldwin - Lomax Turbulence Model

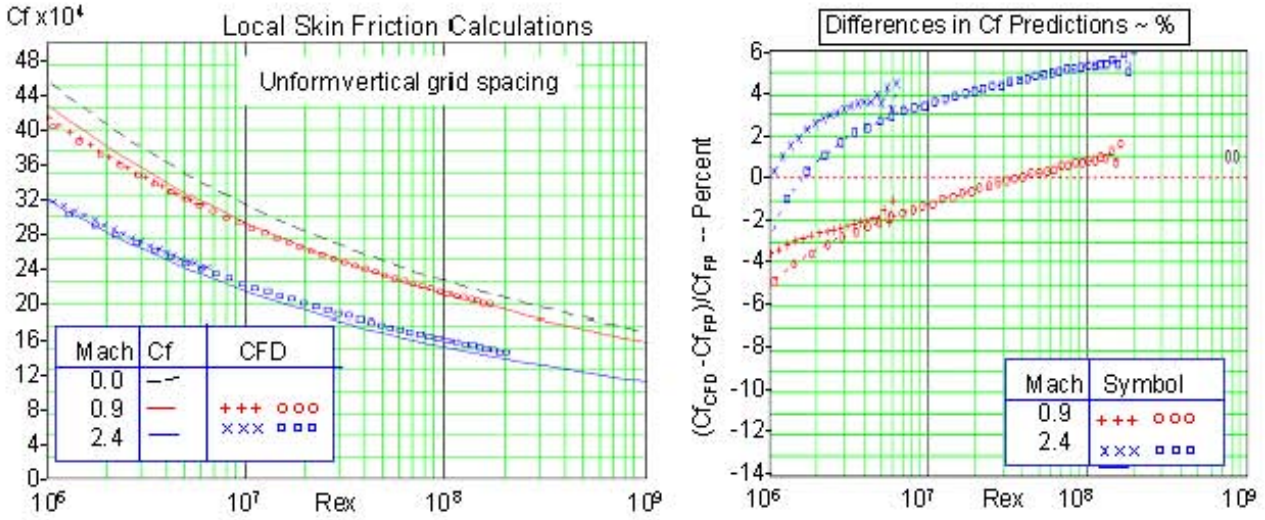

Figure 40 BCAG OVERFLOW: Local Skin friction Calculations; Spalart - Allmaras Turbulence Model

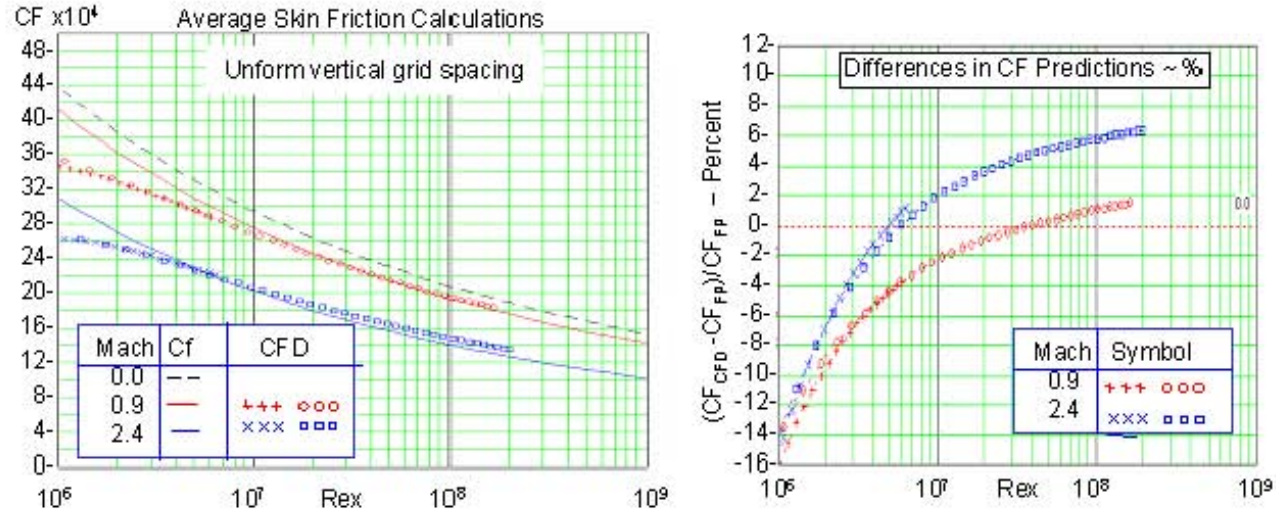

Figure 41 BCAG OVERFLOW: Average Skin friction Calculations; Spalart - Allmaras Turbulence Model

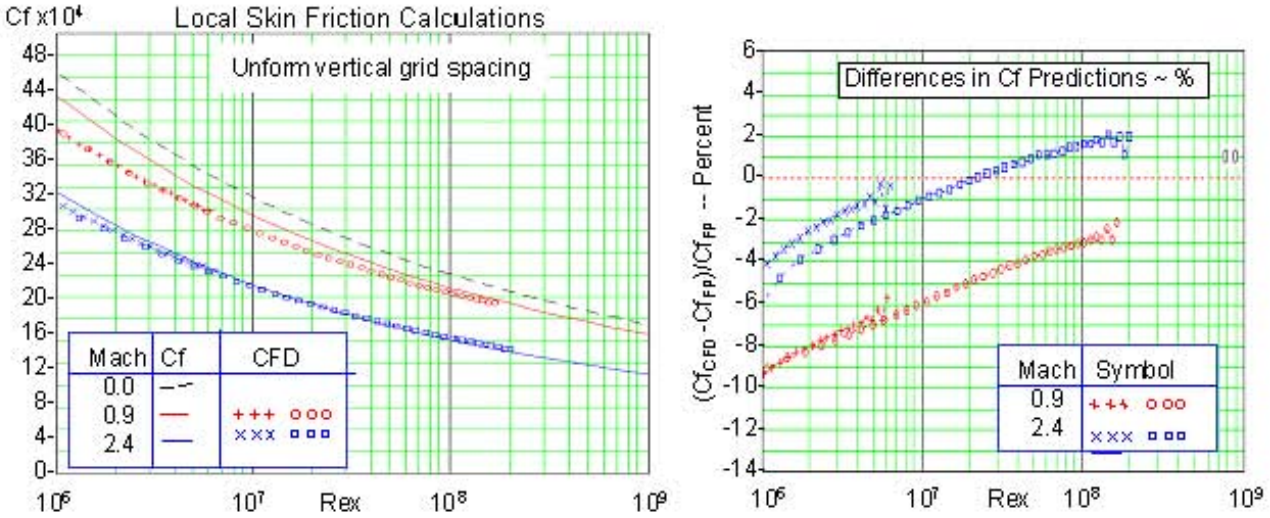

Figure 42 BCAG OVERFLOW: Local Skin friction Calculations; Menter's Turbulence Model

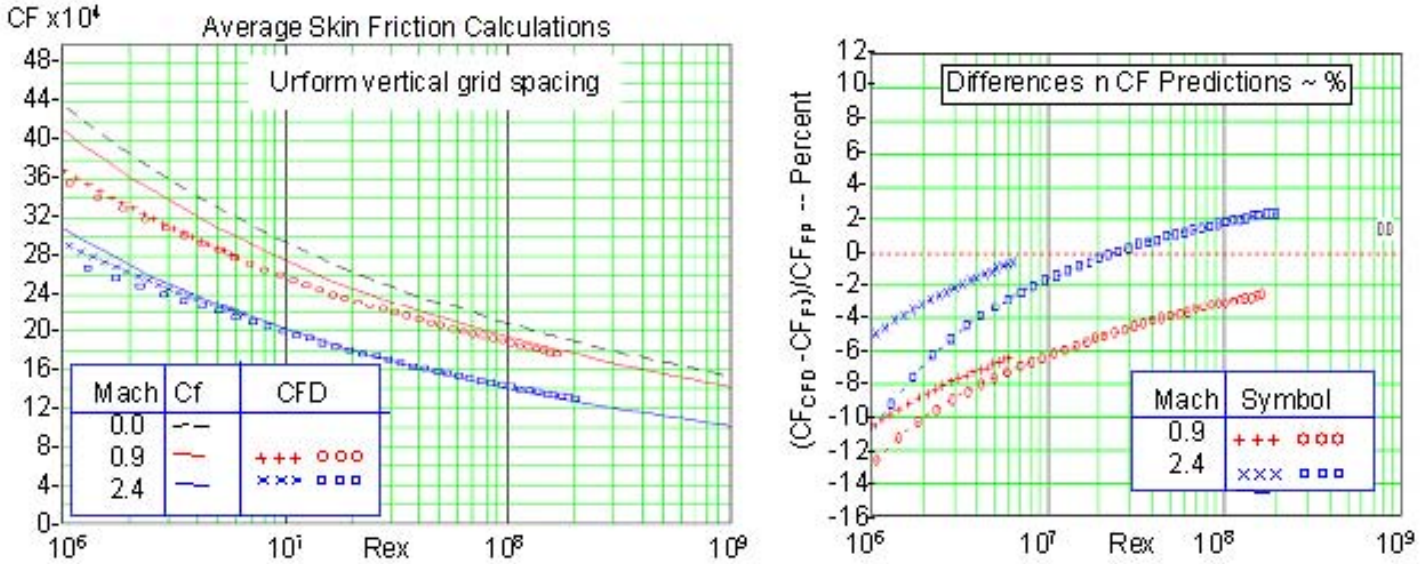

Figure 43 BCAG OVERFLOW: Average Skin friction Calculations; Menter's Turbulence Model

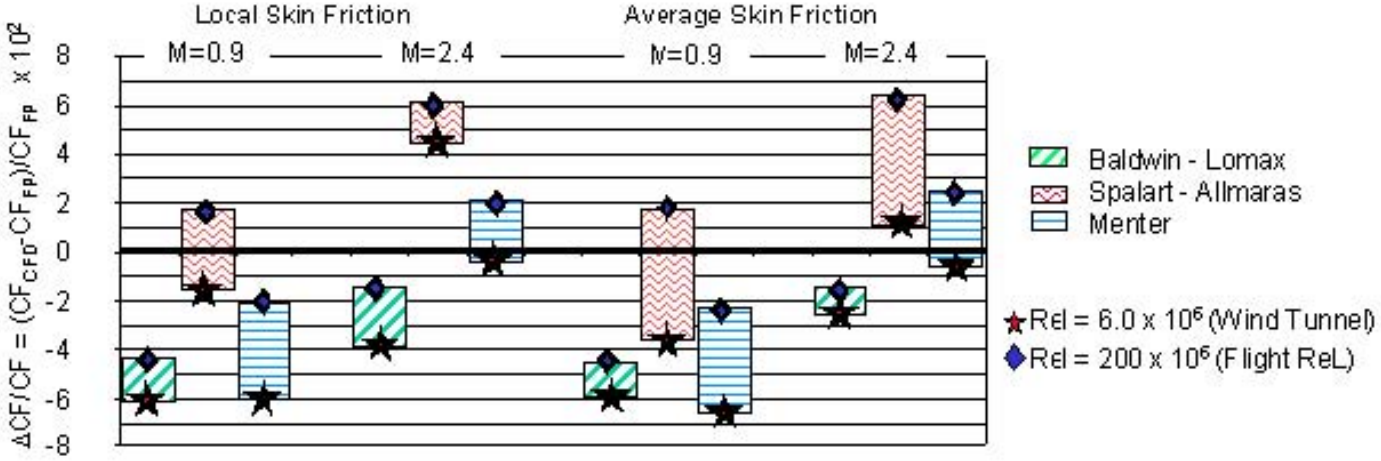

Figure 44 BCAG OVERFLOW: Skin Friction Calculations Comparisons

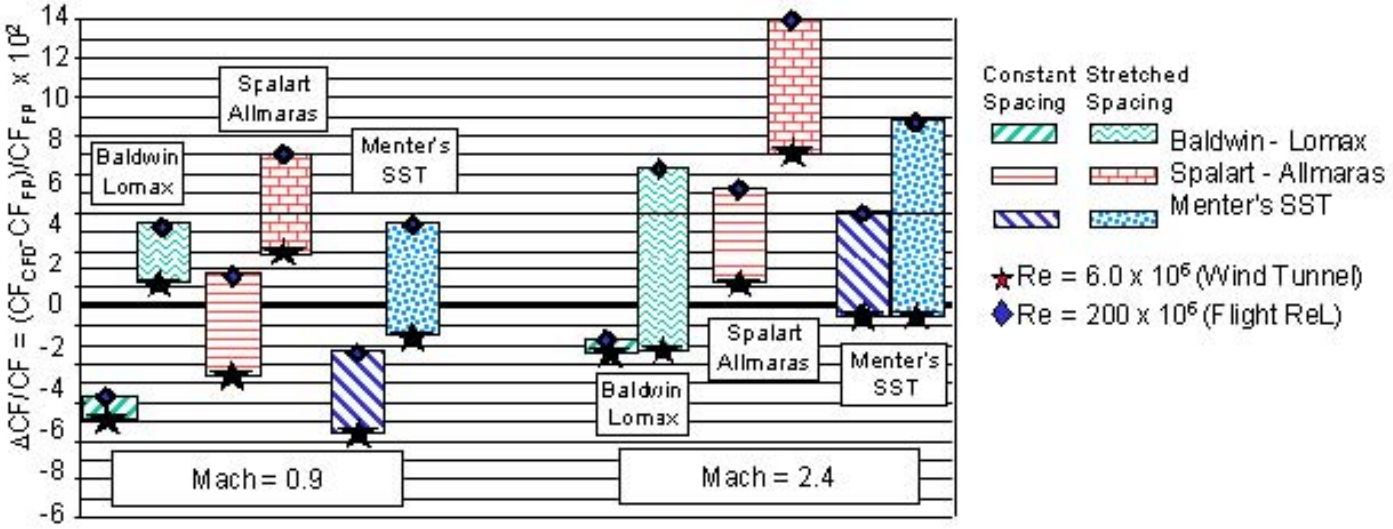

Figure 45 BCAG OVERFLOW: Effect of Grid Spacing on Average Skin Friction

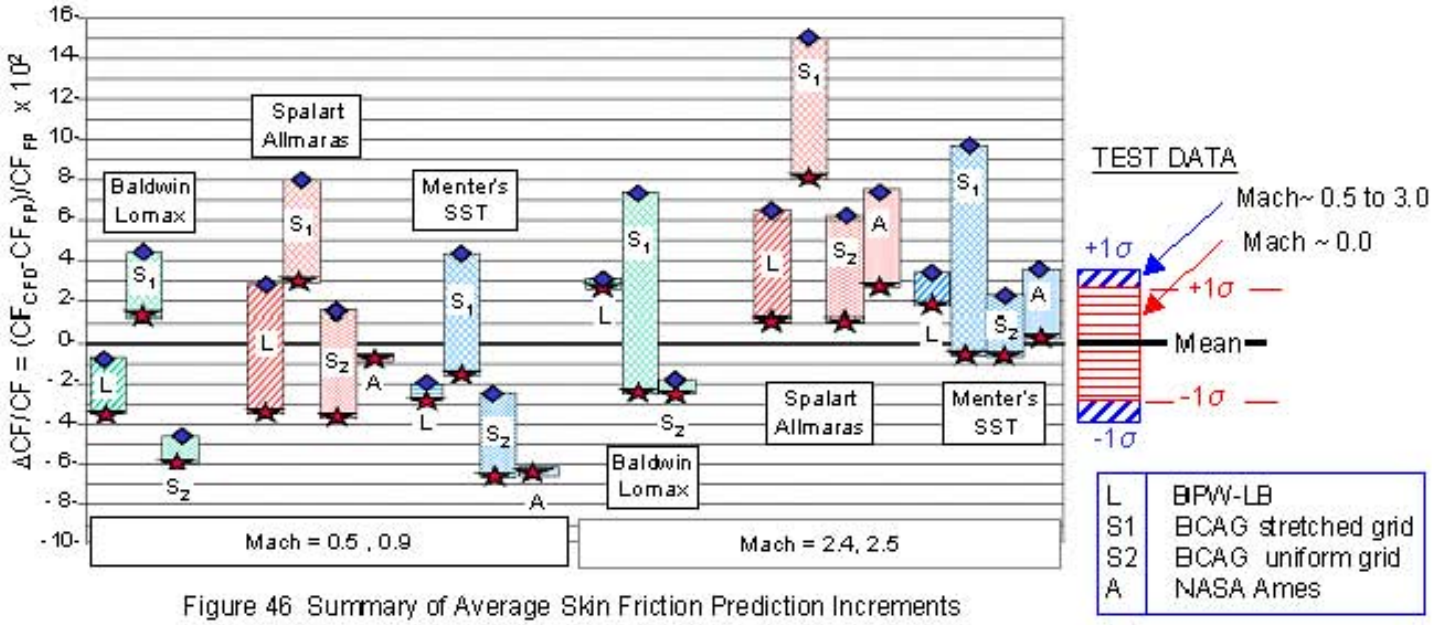

Figure 46 Summary of Average Skin Friction Prediction Increments

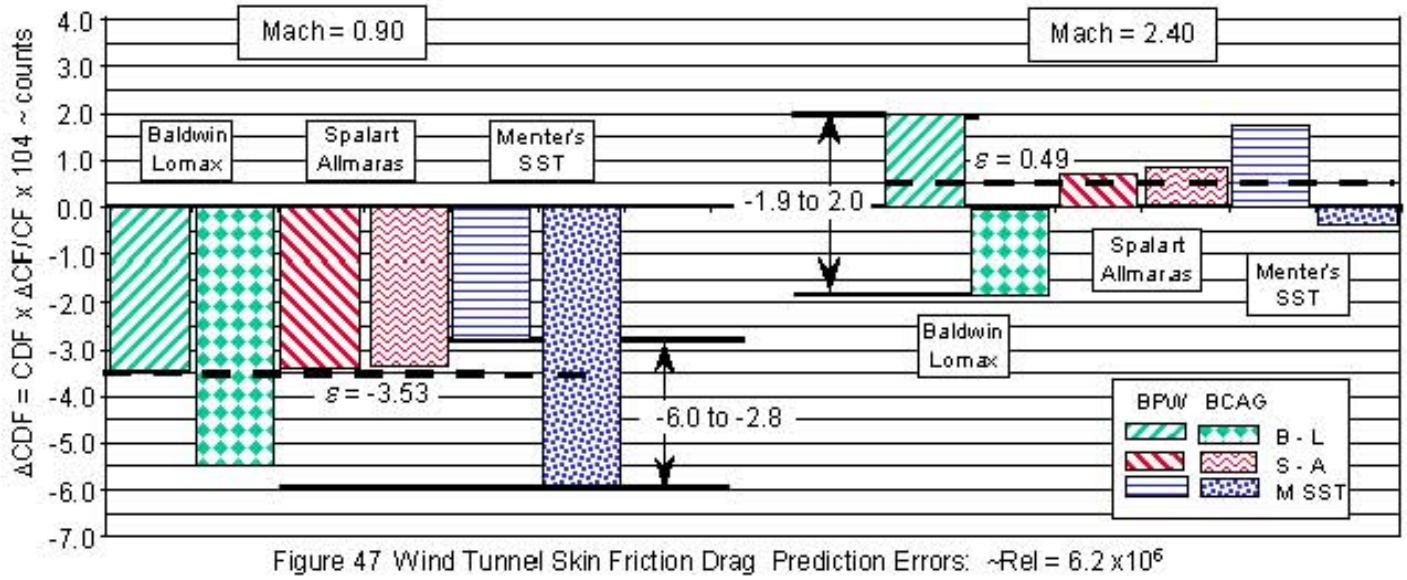

Figure 47 Wind Tunnel Skin Friction Drag Prediction Errors: ~Rel = 6.2 x10^6

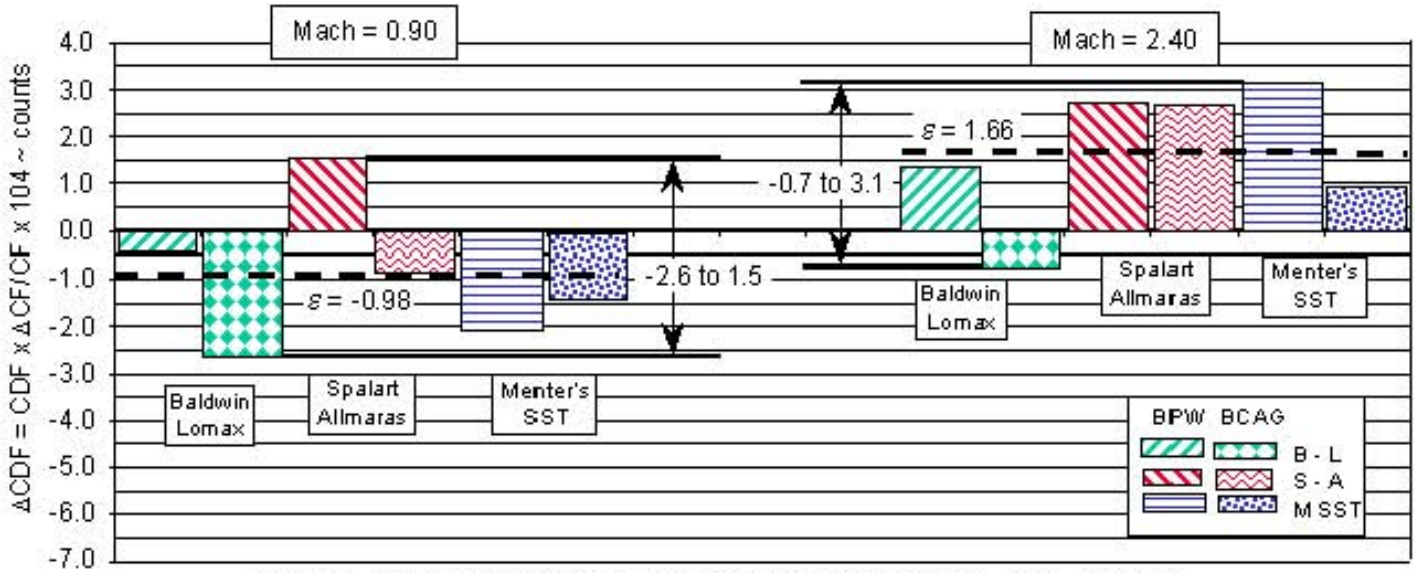

Figure 48 Full Scale Flight Skin Friction Drag Prediction Errors: ~Rel = 180 x10^6

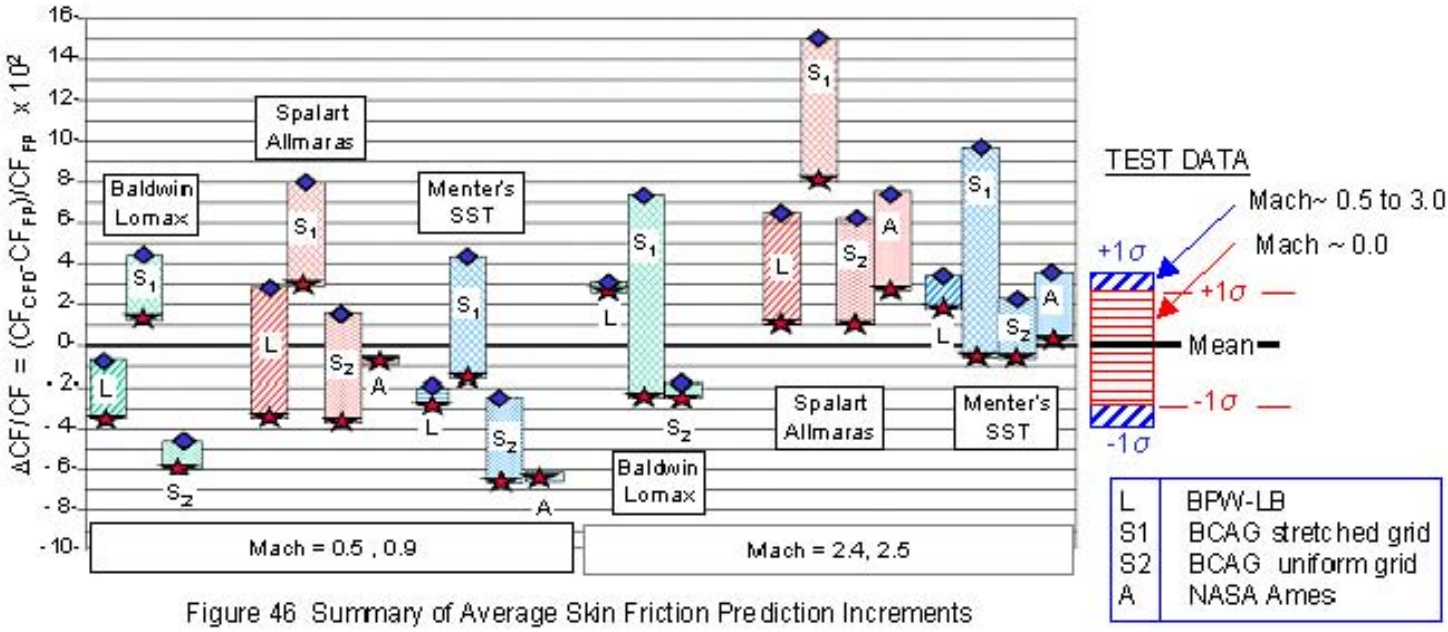

Figure 46 Summary of Average Skin Friction Prediction Increments

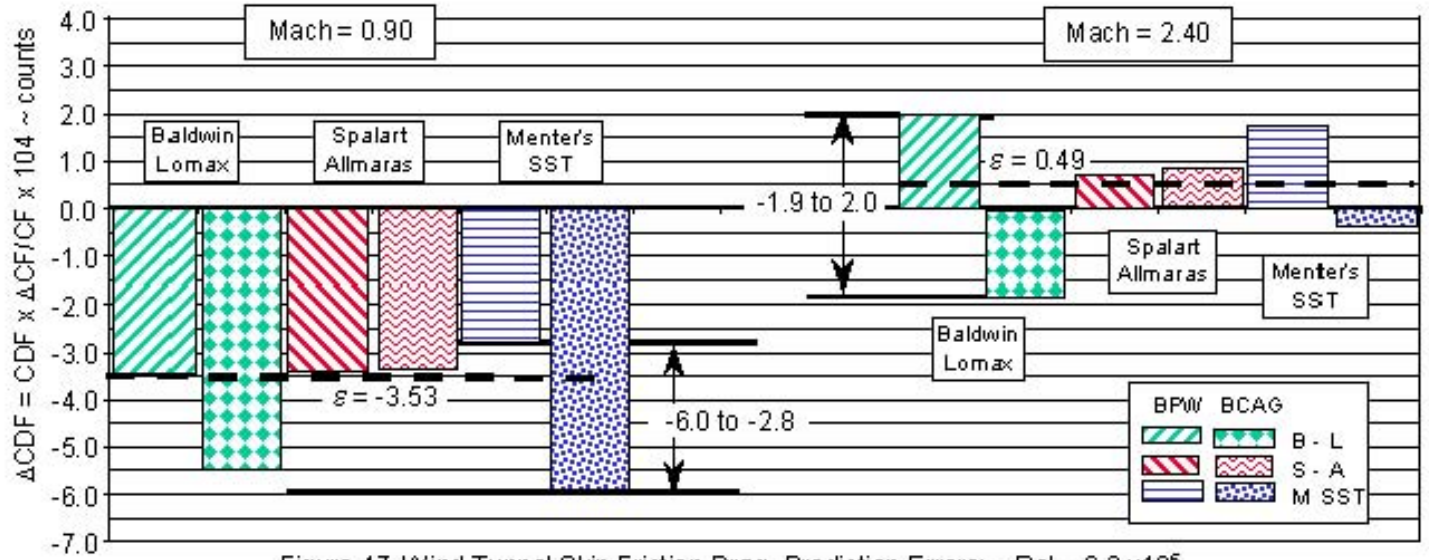

Figure 47 Wind Tunnel Skin Friction Drag Prediction Errors: ~Rel = 6.2 x10^6

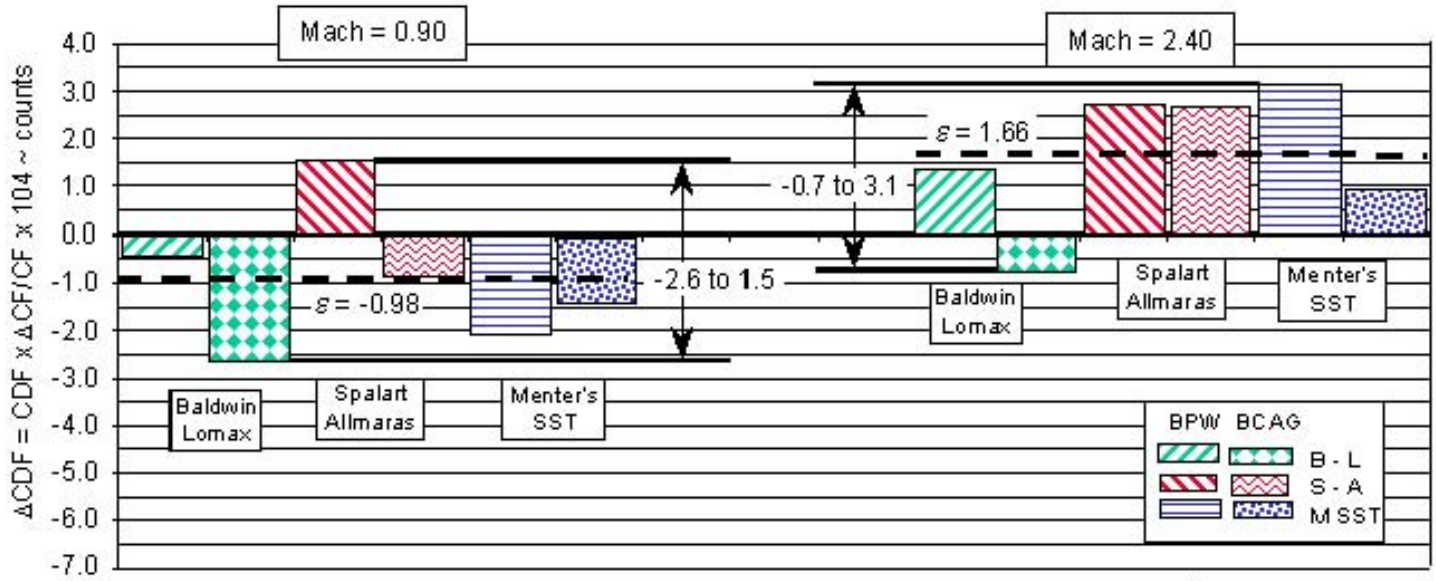

Figure 48 Full Scale Flight Skin Friction Drag Prediction Errors: ~Rel = 180 x10^6

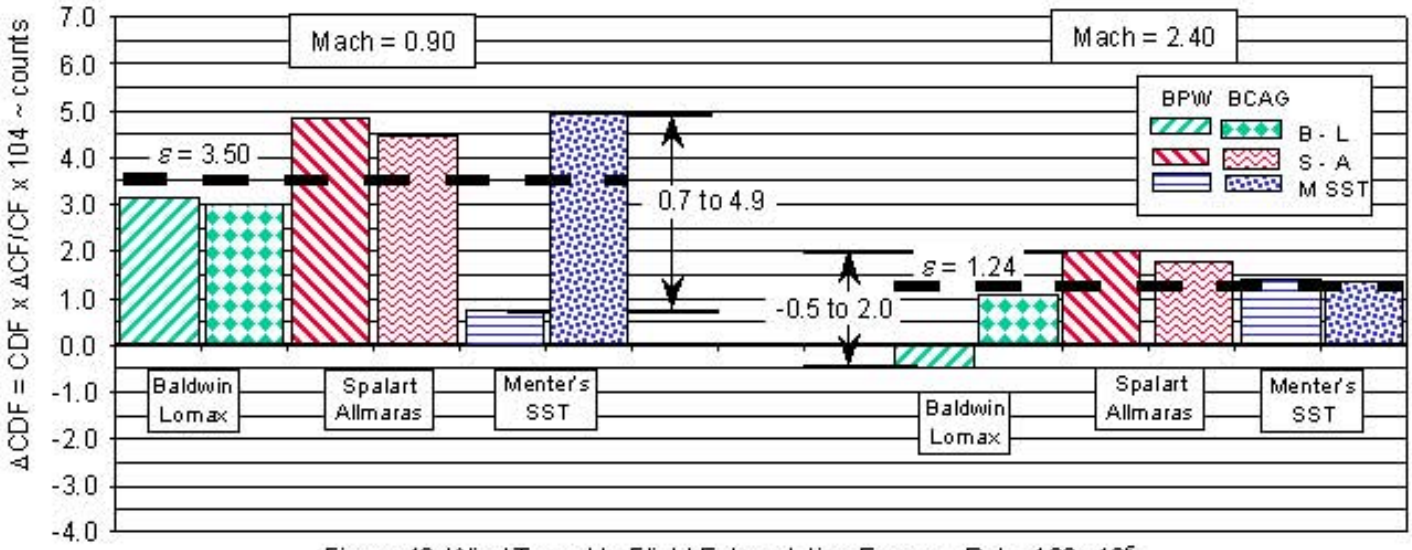

Figure 49 Wind Tunnel to Flight Extrapolation Errors: ~Rel = 180 x10^6